



Project of Strategic Interest NEXTDATA

Special Project RECCO

Deliverable D2.5.R.1b

includes the internal RECCO Deliverable P4.3.1

**Critical issues for meteorological simulations with high resolution
in very complex topography**

WP Coordinator: Silvio Gualdi
CMCC

Authors:
A. Balanzino, S. Trini Castelli
CNR – ISAC, Torino

Introduction

As highlighted in NextData Project, mountain regions are considered as “sentinels of change”, therefore it is a major issue to perform meteorological and climatological simulations that can be accurate enough to correctly represent the atmospheric and environmental processes in such complex topography. For simulations of the meteorological conditions in the mountainous areas, the main choice are mesoscale models, simulating the atmosphere at horizontal scales ranging from a few kilometres to several hundred kilometres, with a typical grid resolution down to the order of 1 km. The main advantage of this kind of models in highly inhomogeneous terrain is their ability to effectively account for the influences of topography on the flow field, resolving valley and slope winds. Mesoscale models are usually driven by the meteorological fields obtained from global models (such as the *European Centre for Medium Range Weather Forecast*, ECMWF, and the *National Centers for Environmental Prediction*, NCEP, analyses), representing the synoptic-scale influence. At the same time, thanks to the grid-nesting technique, they can run with horizontal resolutions high enough to reproduce also the main features of the local meteorology.

Several studies (Gohm et al., 2004; Heimann et al., 2007; Schicker and Seibert, 2009; Trini Castelli et al., 2004 and 2011; Arnold et al., 2012) proved that in highly complex orography certain terrain-induced meteorological processes cannot be captured until 1-km or finer resolutions are used.

In this framework, running high-resolution simulations in the very complex orography of Hindu-Kush Karakorum, Himalaya and Alpine regions allows addressing the following main objectives:

1. to perform a sensitivity analysis for identifying the key physical and numerical issues which are fundamental to improve the reproducibility of the meteorology, and therefore the climatology, in such complex topography;
2. to establish focused benchmark studies for the validation of non-hydrostatic atmospheric circulation models in highly complex topography, providing archives of data for the comparison between predicted and observed meteorological fields.
3. to characterize the local meteorology for identifying locations of specific interest where to install measuring stations.

The simulations are performed with the RAMS (Regional Atmospheric Modeling System, Pielke et al., 1992; Cotton et al., 2003) model. RAMS is a non-hydrostatic model, originally developed from a mesoscale model and a cloud model at the Colorado State University. It represents one of the most developed computational systems in atmospheric numerical modelling, being continuously improved through multidisciplinary work carried at research institutions all over the world. RAMS is designed to simulate a large range of atmospheric flows in a wide spectrum of scales, from local and regional to synoptic. It may be configured to cover an area as large as a hemisphere or to simulate microscale phenomena, since there are no lower limits in the domain size or in the model grid cell size. The model includes a large number of options for the simulation of the atmospheric processes. The main features are hydrostatic and non-hydrostatic mode, two-way interactive grid nesting, terrain-following coordinates, stretched vertical coordinates, nudging system, different options for numerical schemes, several upper and lateral boundary conditions and a set of parameterisations for physical processes. The two-way nesting provides a “zoom” from a large-scale area to smaller scale domains, and the non-hydrostatic option allows to represent all meteorologically relevant spatial scales. RAMS includes a model for soil and vegetation temperature and moisture. In the latest version of RAMS (RAMS6.0) in alternative to the traditional terrain-following coordinates the ADaptive APerture (ADAP, Walko and Tremback, 2002) approach can be used. In this case, the grid structure is a true Cartesian grid where the apertures of the grid cell faces are adapted to topography that would block the flow. The ADAP technique allows dealing with arbitrarily steep and even overhanging

topography, enabling simulations with very high resolution. Together with this, in past years alternative turbulence closure models were implemented and tested in RAMS by our group (Trini Castelli et al., 1999 and 2001; Ferrero et al., 2001 and 2003; Trini Castelli et al. 2004, 2005 and 2006; Alessandrini et al., 2005; Reisin et al, 2007; Trini Castelli and Reisin, 2009 and 2010), in order to provide a better description of the flow structures at high resolution in complex terrain.

In the first phase of RAMS modeling activities, a thorough review of the specialized literature on high resolution simulations in highly complex terrain has been conducted. This allowed identifying the critical aspects of performing simulation of the atmospheric circulation in very inhomogeneous topographical conditions. In this report, the main thematic areas that need assessment are described and discussed in Section 1, where illustrative examples supporting the analysis are presented referring to simulations in the European Alpine areas. In a following stage, described in Section 2, preliminary simulations have been run on the HKKH area to investigate the critical issues in such complex orography, for a critical episode related to a flood (House et al., 2011; Galarneau et al., 2012; Trenberth, 2012; Wang, 2012).

We note that all results are presented in UTC hours. This has to be accounted for when discussing the local daily cycle depending on the season and on the location, corresponding to one or two hours more in local time in the Alpine region and five hours more in the HKKH local time.

1. Review of the critical aspects of meteorological simulations in highly complex terrain.

In this Section a resume of the most critical issues when using meteorological models in complex terrain is discussed. The outputs from past RAMS simulations performed in the Italian Alpine regions for different case studies have been collected and analysed with the specific aim of illustrating these aspects. In particular, here we present examples from meteorological simulations performed in the area of Frejus transect (Trini Castelli et al., 2011) in the Italian and French western Alps, focusing on the comparison between the model predictions and observations at the available surface stations.

It is worth reminding some general considerations for a proper understanding of this kind of comparison. First of all, model outputs are volume averages defined by the horizontal and vertical grid resolutions Δx , Δy , Δz used in the simulated domain and they refer to mean quantities, while the corresponding observations are instantaneous and single-point values that may significantly differ from the averages. In addition to this, the measuring sites are generally in heterogeneous areas that can be not fully resolved at the grid scale, in particular because in complex terrain the orography used in the simulations is generally smoother than the real orography, so that the altitudes of the measuring point and the simulation grid points may be significantly different. This aspect is thoroughly discussed in Section 2. Therefore, due to the smoothed nature of the simulation results, the finer structure in the observed profiles cannot be fully captured.

On their side, the observed meteorological variables are affected by fundamental stochastic uncertainty: according to many authors and to our experience too, a variability of hourly averaged wind speed of the order of 1 - 2 ms^{-1} over distances of a few kilometres can be observed even on flat homogeneous terrain, due to mesoscale turbulence fluctuations. Moreover, instrumentation and averaging errors, unavoidable in any measurements, can affect this kind of paired comparisons. For all these reasons, a precise point-to-point agreement between observed and predicted data cannot be expected and a good result is obtained when the mean trend of measurements is reproduced by the simulated variables.

In general, to produce the simulated fields at a surface station, it is possible to interpolate on its location the values simulated at the grid points surrounding it, possibly applying also a vertical interpolation from the closest model levels to the height of the site. Since we are dealing with highly complex topography and land use heterogeneity, in the examples we plot the predicted data of the first model level (about 24 m high) at the four grid points around the station, in order to highlight the possible differences due to the different altitudes of the points.

Simulation outputs were available for three periods:

- one summer episode: 3 - 13 July 2004;
- two winter episodes: 10 - 20 December 2004 and 8 - 18 February 2004.

For every period, the comparisons are performed at several stations in urban centres and villages in the two valleys: Turin, Susa, Salbertrand, Bardonecchia for the Susa valley and Mont Cenis, Modane, St Michel de Maurienne and St Marie de Cuines for the Maurienne valley. The surface station generally provide wind velocity measured at 10 m and temperature at 2 m above the ground or, when the mast is located over a roof, as in urban sites, at higher heights (for instance, in Turin at a height typically of 30 m).

In RAMS the two-way nesting procedure was applied and the simulation was configured using four nested grids (Figure 1.1): the main outer one covers a domain of 1000 x 1000 km, where the main large scales topographical features of North Italy and South France, till the Pyrenees and the Northern Mediterranean Sea to the West, and all the Alpine arc from West to East, are included. The next two intermediate grids zoom over the area of interest and they are chosen to be compatible with the main local topographic features. The finest domain, having the highest resolution, is focused over the Frejus area. In the vertical, a

stretched grid is used, with the highest resolution of about 24 m (first model level) at the surface. The 3D configuration of the grids are:

Grid 1: 1088 x 1088 x 17 km with a horizontal grid mesh of 64 x 64 km

Grid 2: 592 x 464 x 17 km with a horizontal grid mesh of 16 x 16 km

Grid 3: 196 x 132 x 17 km with a horizontal grid mesh of 4 x 4 km

Grid 4: 133 x 61 x 17 km with a horizontal grid mesh of 1 x 1 km.

As it can be seen from Figure 1.1, with a resolution of 4 km and 1 km the details of the topography definition improves with respect to the larger domains and it is possible to better characterize the main Alpine range in the territory.

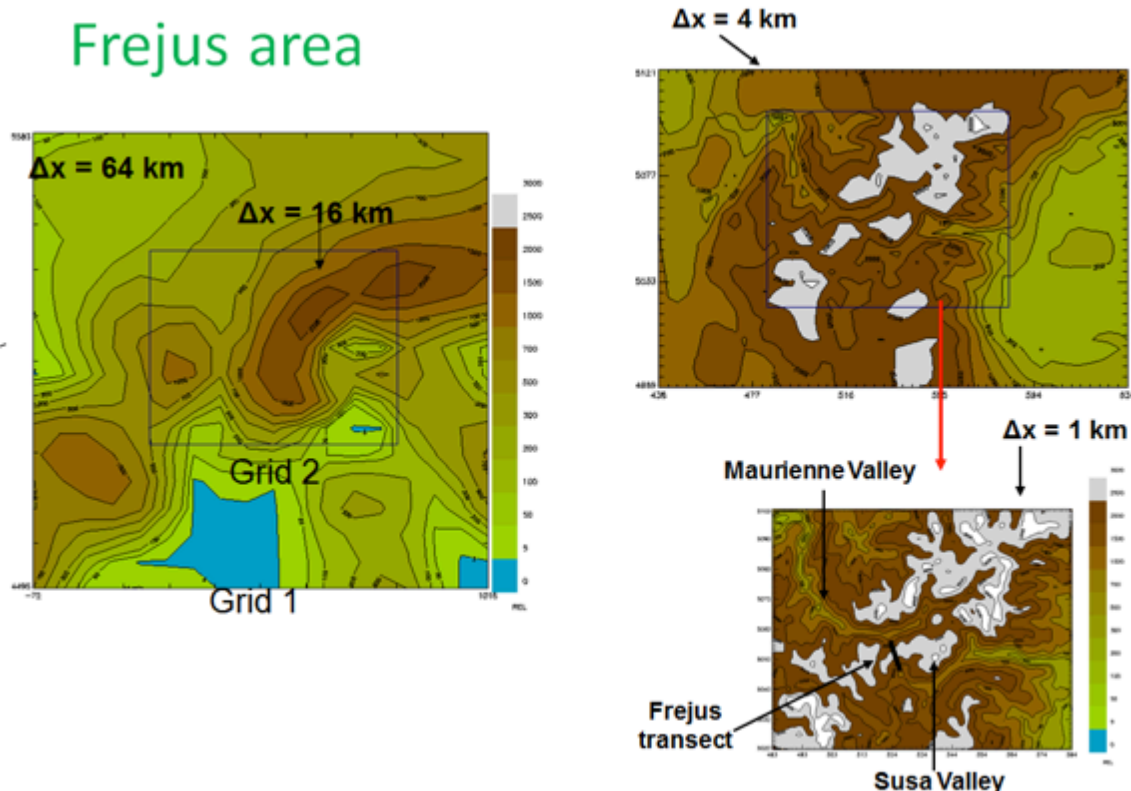


Fig. 1.1. Domains and orography contours of the four RAMS nested grids for the Italian-French Frejus Alpine transect.

1.1 Grid resolution

As anticipated in the introduction, several studies in real complex terrain demonstrated that typical terrain-induced meteorological processes cannot be correctly captured when using resolutions coarser than 1 km or even less. Already at resolutions of 3-4 km, model forecasts can happen to deviate substantially from the observations. In Figure 1.2 and 1.3 a couple of illustrative comparisons between predicted and observed variables are plotted for February and July periods at two stations: Susa (520 m a.s.l) and Bardonecchia (1353 m a.s.l), where detailed measurements were available, for the two smallest grids, Grid 3 and 4.

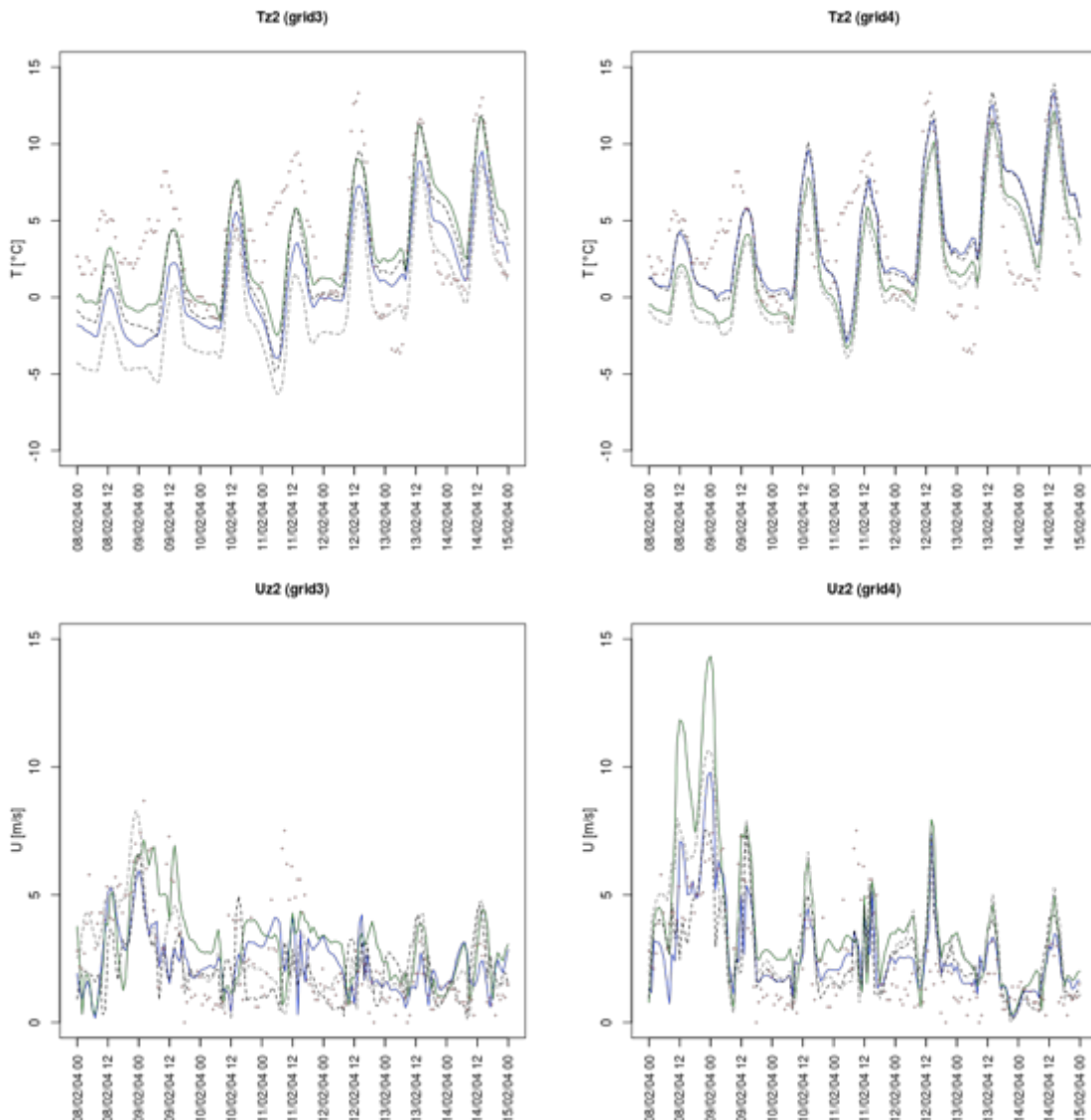


Fig. 1.2. February run, Bardonecchia station (1353 m alt). Comparison of observed (red crosses) with predicted temperature (top) and wind speed (bottom) for Grid 3 (left) and Grid 4 (right), at the first model level of four grid points around the station. Grid points altitudes: GRID 3: SW 1811 m (blue solid line), NW 1687 m (green solid line), SE 1603 m (blue dashed line), NE 2078 m (green dashed line); GRID 4: SW 1422 m (blue solid line), NW 1448 m (green solid line), SE 1626 m (blue dashed line), NE 1700 m (green dashed line).

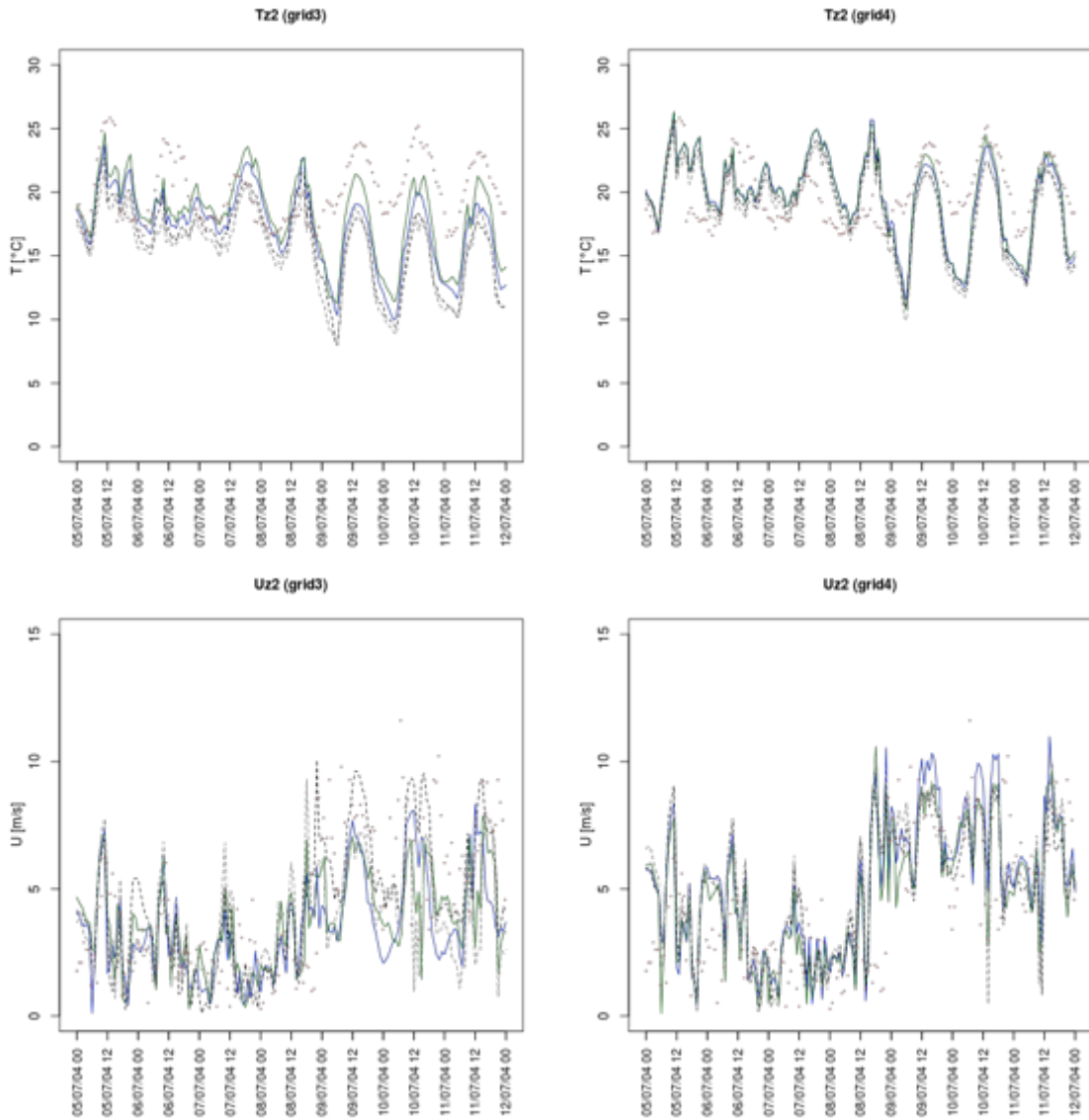


Fig. 1.3. As in Figure 1.2, but for July run and Susa station (520 m alt). Grid points altitudes: GRID 3: SW 968 m (blue solid line), NW 1161 m (green solid line), SE 827 m (blue dashed line), NE 1220 m (green dashed line); GRID 4: SW 607 m (blue solid line), NW 709 m (green solid line), SE 599 m (blue dashed line), NE 764 m (green dashed line).

The agreement is relatively good for both grids but the spreading of the curves at the four points reduces in Grid 4 thanks to the finer resolution, with the altitudes of the grid points being closer to the site one, thus more representative of the local features. Connected to the sensitivity to grid resolution, a problem may arise when comparing predicted and observed data at measured stations by interpolating the values obtained at surrounding grid-points. While this approach can be acceptable in homogeneous terrain, as noted before it becomes not straight applicable in complex orography since values at rather different altitudes might be improperly interpolated. Therefore, when there is the need to obtain variables interpolated on the location of a measuring station, having finer grids makes the comparison more reliable.

Modelling systems generally offer their own post-processing packages to extract variables at stations or given points. In RAMS, through a so-called 'GRAB' option the coordinates of the station/point of interest are reported on the grid domain in metre units, the grid points

surrounding it are identified and variables are linearly interpolated both horizontally and vertically to provide their predicted values.

In Figure 1.4 and 1.5 scatter plots of the predicted and observed variables are plotted respectively for the February and July periods at Susa and Bardonecchia stations for Grid 3 and Grid 4. In this case, to obtain paired values, the predicted variable is interpolated from the surrounding points through RAMS GRAB facility. The general improvement of the agreement for Grid 4 is appreciable, in particular for the temperature, but the data interpolation is a critical issue, as discussed in more details in next Section 2.1.

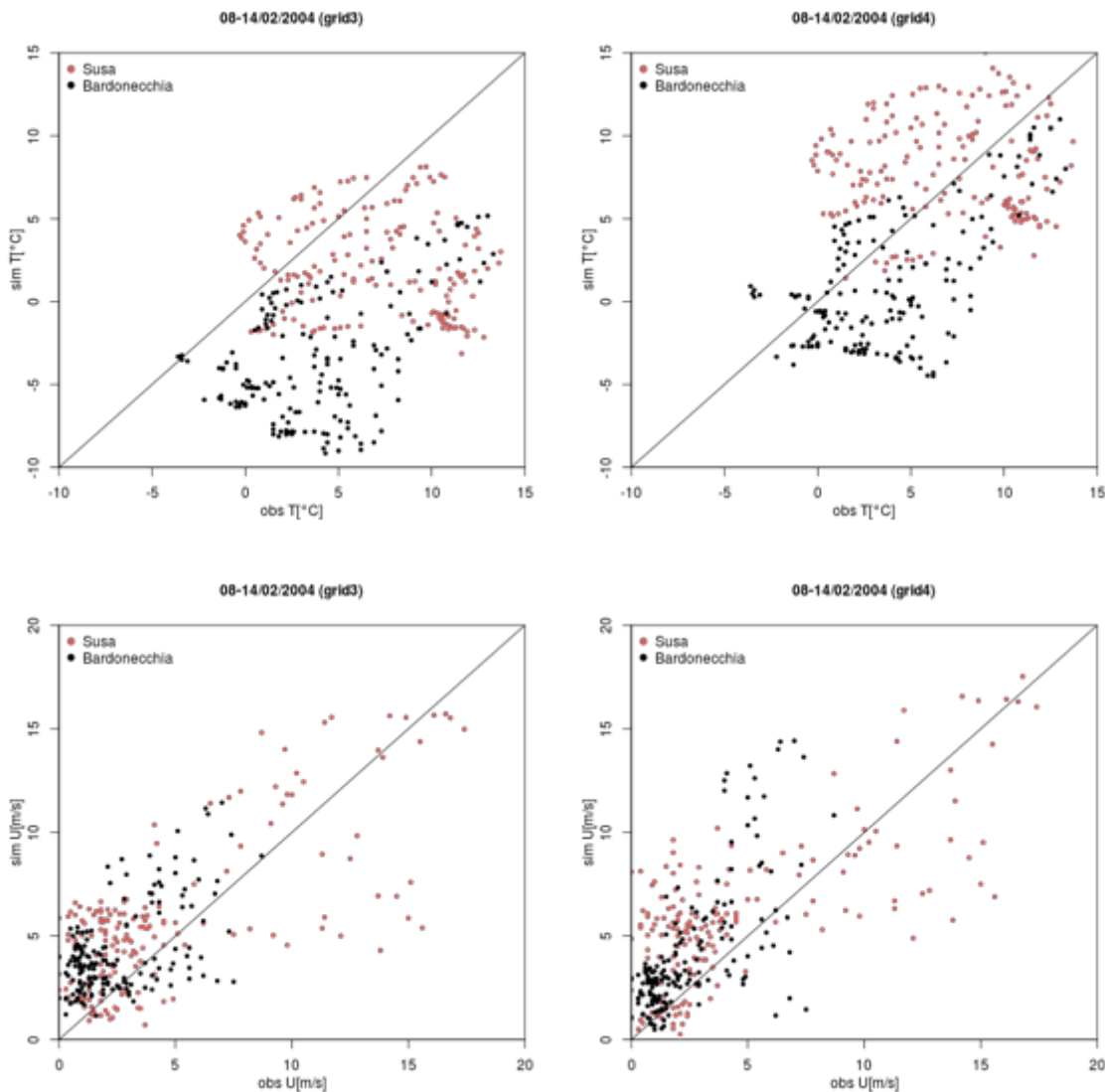


Fig. 1.4. February run. Scatter plots of the temperature (top) and wind speed (bottom) at Susa (red points) and Bardonecchia (black points) stations for Grid 3 (left) and Grid 4 (right).

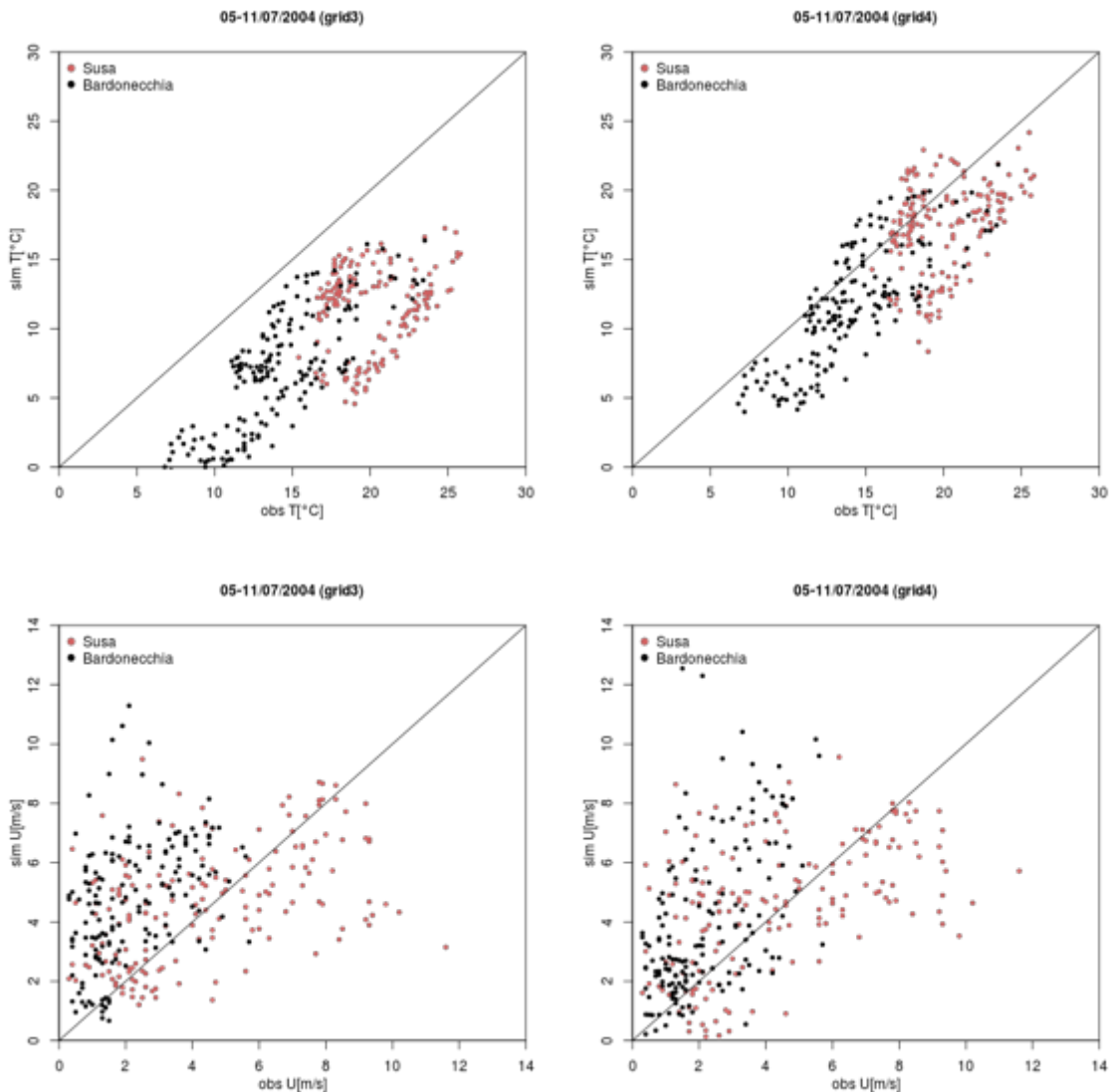


Fig. 1.5. As in Figure 1.4 but for July run.

This can be highlighted by comparing the trends of the interpolated variables, in Figures 1.6 and 1.7, with the four-point graphs plotted in Figures 1.2 and 1.3. The agreement results to be better for Grid 4 especially for the temperature, as can be expected. However, the interpolated lines in Figures 1.6 and 1.7 show an agreement with the observations even worse than the worst case when looking at the four surrounding points.

The four points in Figures 1.2 and 1.3 correspond to the grid points of the grid cell where the station is included and are selected directly checking their longitude and latitude with respect to the station ones. We notice that when extrapolating the variables from RAMS outputs with the GRAB option, using the longitude and latitude of the measuring station, the final model points extracted for the comparison are displaced with respect to it, therefore possibly spoiling the correctness of the comparison itself. In the RAMS case, this can be ascribed to the passage from the geographical system to the coordinates in metres that is used for GRAB option, possibly leading to an incorrect final positioning of the points to be interpolated, and to the vertical interpolation, not used in Figure 1.2 and 1.3 since the first RAMS level is considered. In Table 1.1, we report as an example the coordinates of the stations compared to the model extracted points of Figures 1.6 and 1.7. These results lead to a warning, which is to treat with particular care the comparison between observations and predictions from model simulations

especially in complex terrain, to avoid misinterpreting the results and to assure that correct conclusions are drawn.

Table 1.1. Coordinates of the measuring stations compared to those of the points extracted through an interpolation from RAMS outputs.

		Real coordinates	Grid 3 point	Grid 4 point
Susa	Lon	7.055°	7.05566°	7.05516°
	Lat	45.1428°	45.179°	45.1518°
	Alt	520 m	1806 m	962 m
Bardonecchia	Lon	6.7175°	6.76895°	6.73024°
	Lat	45.0758°	45.1115°	45.0757°
	Alt	1353 m	2422 m	1851 m

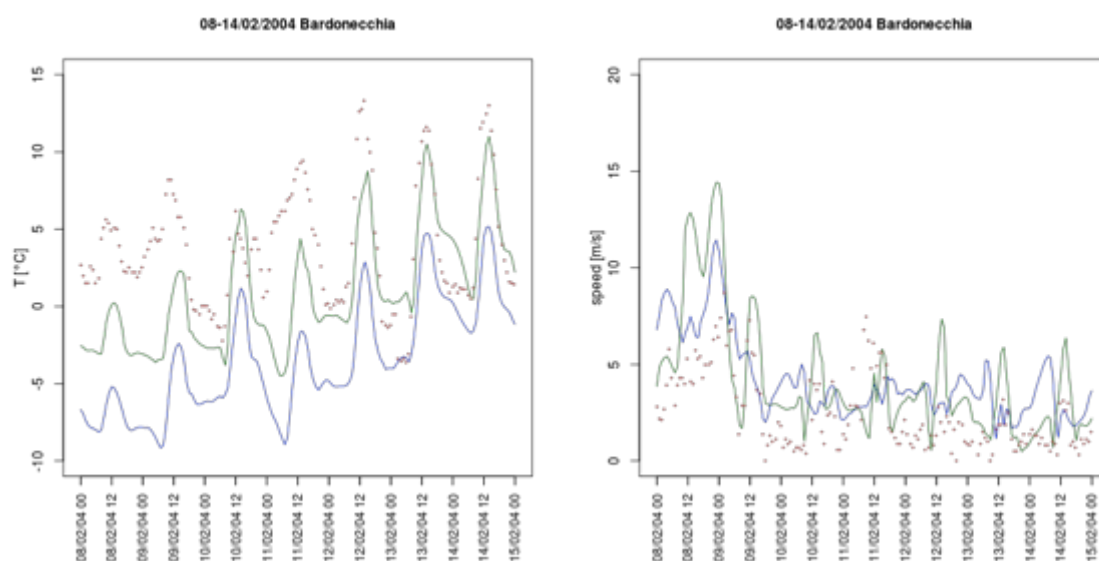


Fig. 1.6. February run, Bardonecchia station (1353 m alt). Comparison between interpolated predicted variables for Grid 3 (blue line) and Grid 4 (green line) and observations (red crosses), temperature (left) and wind speed (right).

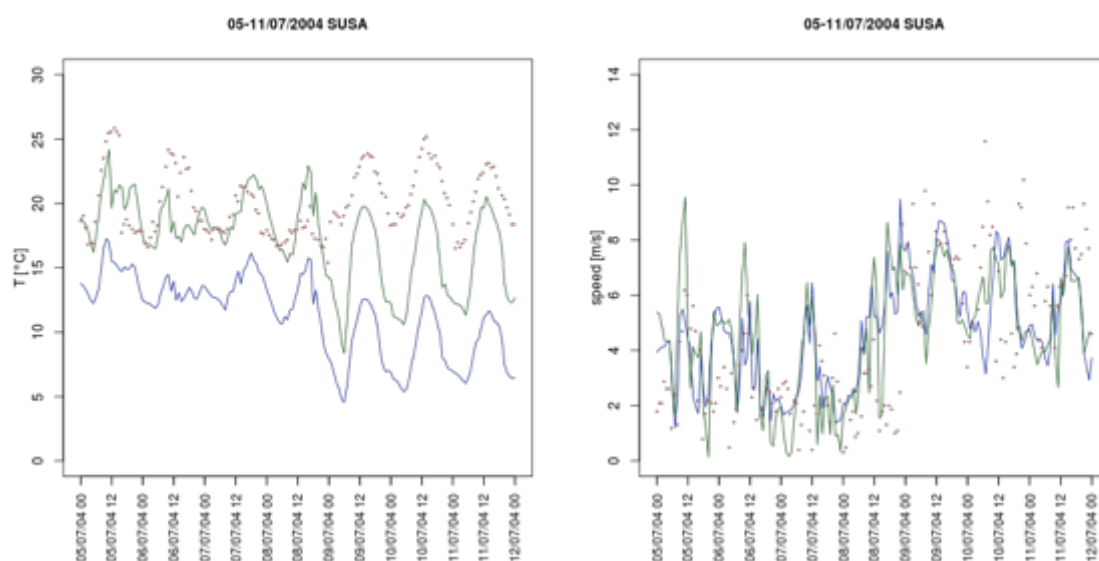


Fig. 1.7. As in Figure 1.6 but for July run and Susa station.

1.2 Boundary layer parameterizations

The parameterizations for boundary layer and surface exchange used in mesoscale models are based on hypotheses and approximations for atmospheric turbulence that are generally valid for homogeneous and flat terrain, as in Monin-Obukhov similarity theory. Often they are derived in 'optimal' conditions, as neutral or weakly stable/unstable stratification and near-steady-state flows. When dealing with complex topography, these parameterizations may come to their limit of applicability, especially using high resolutions. In particular, it has been proven that the turbulence closure models, commonly implemented in mesoscale models, work well until grid sizes of the order of 1 km, where their reliability starts being questionable (Morton and Molders, 2007; Stevens et al., 2010; Morton et al., 2009, 2010a, 2010b, 2010c).

As summarized in Arnold et al. (2012) for high resolution modelling, mesoscale models adopt two different approaches to solve the prognostic equations for the mean flow and parameterize the turbulence:

- Reynolds-Averaged Navier-Stokes, *RANS*, approach: an *ensemble-averaging approach*, where the Navier-Stokes equations are decomposed into their mean and fluctuation parts following Reynolds decomposition, then they are ensemble-averaged. In this case, turbulence is fully parameterized, the variances and co-variances of turbulent quantities are expressed as functions of the mean flow variables.
- Large Eddy Simulations, *LES*, approach: the Navier-Stokes equations are filtered with a filter length characteristic of the inertial sub-range of the turbulence spectra. The model resolves the large eddies and the small-scale isotropic turbulence is parameterized.

At present, mesoscale RANS models are still mostly used for simulations in real complex terrain, therefore we focus the discussion on them. Clearly in complex terrain the turbulence structure becomes extremely complicated, due both to mechanical turbulence, produced by the wind interacting with the orography and generating secondary circulations, and to the thermal turbulence, associated to the typical mountain breeze and generating local turbulence induced by the different heating of the mountain slopes.

In Arnold et al. (2012) it is noted that current RANS turbulence schemes “ (...) *only consider vertical turbulent fluxes which are assumed to depend on conditions in a single vertical column of air without accounting for the surrounding topography, whereas turbulent structures in complex terrain are fully three-dimensional. Therefore a new generation of boundary layer parameterizations, accounting for the surrounding topography instead of considering just a one-dimensional column, is needed to realistically represent the turbulence in narrow valleys (G. Zängl et al., 2003)*”.

Another problem is linked to the horizontal resolution: when the grid cells become small, horizontal turbulent fluxes as well as advection of turbulence, i.e. horizontal advection of turbulent kinetic energy, cannot be neglected.

In this framework, Trini Castelli et al. (2001, 2005 and 2006) demonstrated that the *boundary-layer approximation*, for which horizontal diffusion terms are neglected and only vertical gradients are retained, adopted in the Mellor-Yamada model, level 2.5, typically used in mesoscale models (Mellor and Yamada, 1982) can be problematic in complex terrain at resolutions of 1 km. This because the horizontal gradients of velocity induced by the presence of valleys and orographic features are not taken into account, possibly leading to an underestimation of turbulent kinetic energy production and of the horizontal diffusion.

In order to investigate these aspects, the RAMS simulations in the Frejus area were repeated simulating a daily cycle in this real complex terrain, considering different combinations for the calculation of the turbulence. RAMS was run in a configuration with four nested grids, but in this case nesting until 250 m resolution for the smallest grid (Trini Castelli et al., 2008).

Three turbulence closures implemented in RAMS were tested: the widely used Mellor-Yamada 2.5 scheme (Mellor and Yamada, 1974 and 1982, MY2.5 hereafter), a standard E-l isotropic closure (Trini Castelli et al., 2001, 2005) and a so-called “anisotropic version” of the E-l closure (Trini Castelli et al., 2006, El-anis hereafter). The standard E-l closure describes isotropic turbulence, thus it could better represent and solve the flow and turbulence when horizontal resolutions approach the order of ~ 100 m, which is the typical vertical resolution used in the atmospheric boundary layer in mesoscale modelling. On the other hand, non-isotropic closures should be more appropriate for the simulation of the atmospheric processes determined and characterized by non-homogeneous and non-isotropic conditions, and when relatively fine resolutions in the vertical are matched with large resolutions in the horizontal. We briefly recall that MY2.5 scheme solves the turbulent kinetic energy (t.k.e.) equation in the boundary layer approximation, while in E-l and El-anis schemes the dynamical equation of the t.k.e. is fully 3D. In RAMS, MY2.5 is used in the vertical and it is coupled with a Smagorinsky-type (1963) deformational scheme in the horizontal, based on the horizontal deformation of horizontal velocity components and on a length scale, set equal to the horizontal grid spacing $\Delta x = \Delta y$. An analogous combination is adopted for the El-anis scheme, which applies the E-l closure in the vertical and the deformation scheme in the horizontal, but here the full 3D deformation of velocity components is used and the deformation length scale is calculated as $(\Delta x \Delta y \Delta z)^{1/3}$.

The domain of the simulation covers the North-West Italian Alpine region around Turin (Figure 1.8) and the selected simulation period is a summer day, 9 July 2004, characterized by strong convection and high wind velocity. In the numerical simulations, four nested 3D grids are used in RAMS: the largest one has a horizontal resolution of 16 km, the second one a 4 km grid-mesh, while grids 3 and 4 has respectively 1 km and 250 m grid meshes. In the vertical, 26 levels on a stretched grid are used, the first level being at 24 m height and the top of the domain at 16.5 km. The smallest domain is characterized by the presence of both almost flat terrain, around Turin city, and complex terrain, corresponding to the foot of the Alps on the West side and to the hill chain on the East side.

The outputs of the simulations have been here further analysed and as examples of the differences between the turbulence closures and of the effect of the resolution, hereafter some illustrative figures are included.

In Figure 1.9 the histograms describing the distribution of the t.k.e. values for the three turbulence closures are plotted, separating the diurnal (12 a.m. – 11 p.m.) and nocturnal (12 p.m. – 11 a.m.) time periods.

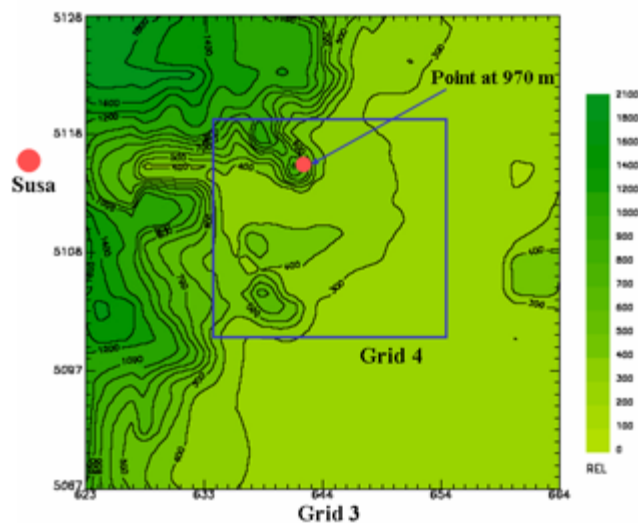


Fig. 1.8. Grids 3 and 4 simulation domains for Turin Alpine area in northwestern Italy.

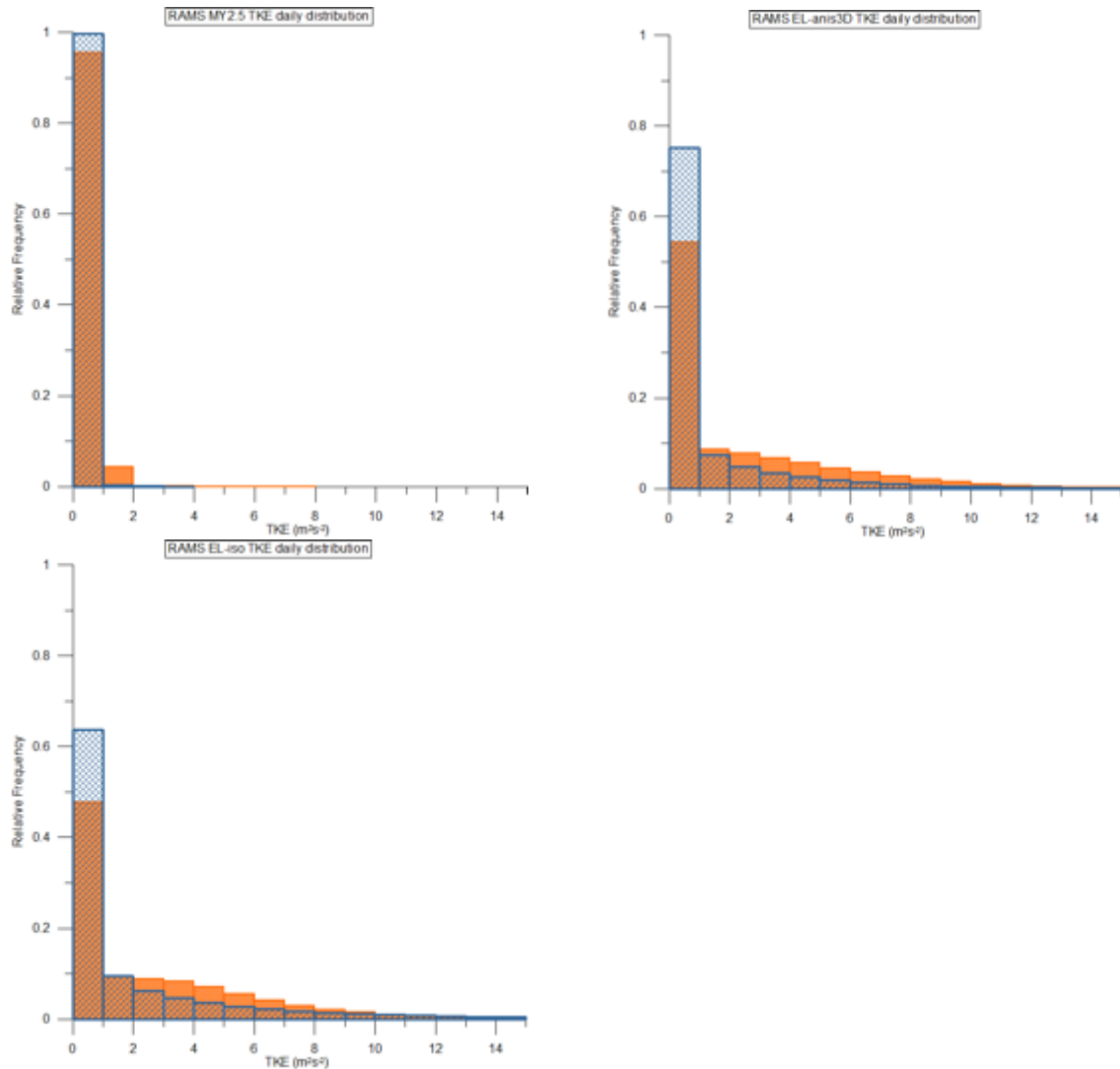


Fig. 1.9. Histograms of the t.k.e. distribution for MY2.5 (top left), El-Anis3D (top right) and El_iso (bottom left) turbulence closures. Orange: diurnal data (12 p.m. - 11 p.m.); blue: nocturnal data (12 a.m. - 11 a.m.).

In general the MY2.5 closure is producing much lower values than El-type closures: more than 95% of the MY2.5 t.k.e. values lay in the range $< 1 \text{ m}^2\text{s}^{-2}$, thus they might be not fully representative of the turbulence conditions determined by high wind velocity, convective conditions and complex terrain as those characteristics of the day considered here. El-type closures, instead, distribute in a larger range and better represent the modulation of the turbulent production in the day. In a few cases, they produce a small percentage of unlikely high values: worst cases occur for E-l run, where the 0.58% of t.k.e. data in Grid 4 get $> 20 \text{ m}^2\text{s}^{-2}$. These values are produced often at the boundaries of the domains and at the nesting boundary, then in correspondence with changing orography, and are probably due to discontinuities in the flow inducing high velocity gradients, therefore high turbulence production. Sometimes, high t.k.e. values occur also at heights over the boundary layer and during the night, probably generated by numerical instabilities when the turbulence quantities, determining the closure scheme, assume low threshold values.

In Figure 1.10 the daily t.k.e. trend at the first RAMS level (24 m) at a point on the slope of the mountain, at 970 m (see Figure 1.8), is plotted for Grid 3 and Grid 4. The trend is, as expected, similar in the two grids, but in the finest Grid 4 the TKE values are generally slightly higher. What is worth to notice is the large difference between the MY2.5 scheme

and the EL-based ones. MY2.5 scheme is producing very low turbulence: this was found to be incorrect when comparing MY2.5 simulations to observed datasets and it was correlated to the boundary-layer approximation adopted in MY2.5 closure (Trini Castelli et al., 2001, 2006). The isotropic version, El-iso, of the E-l closure shows a larger variation in time and in principle cannot be used with confidence when the horizontal and vertical resolutions are too different.

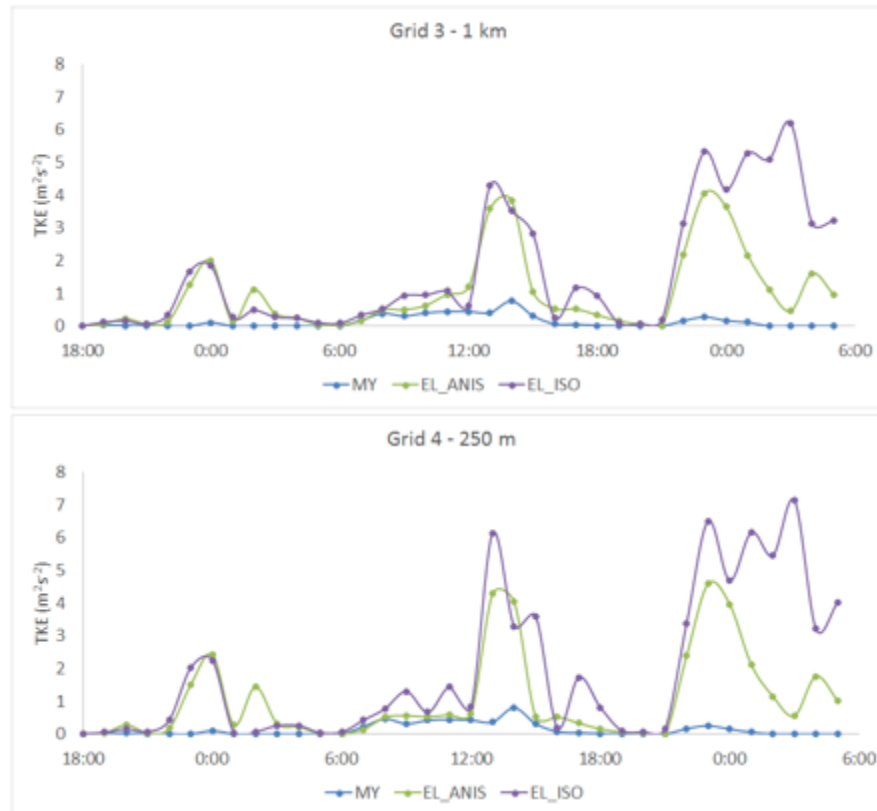


Fig. 1.10. Turbulent Kinetic Energy parameterised with MY2.5 (blue line), EL_anis (green line) and EL-iso (violet line) closures, at a station on the mountain slope, for Grid 3 (top) and Grid 4 (bottom).

We recall also that, when considering high resolutions, thus small grid cells, a larger portion of the turbulent mixing can be explicitly resolved. This implies that using the additional turbulence parameterization might bring to calculate twice part of the turbulent spectrum and it becomes critical and questionable what has still to be parameterized and which are the appropriate closure schemes for such cases. The study of the turbulence structure in complex terrain with mesoscale models is still an open field of research, both on the modelling and on the observational viewpoints.

The concept of “*Terra Incognita*” introduced by Wyngaard (2004) well describes the problematic of dealing with high resolutions. Here, defining l as the energy-containing turbulence scale and Δ as the scale of the spatial filter used on the equation of motions, the two main class of numerical modelling are identified as mesoscale, for $l \ll \Delta$, and LES, for $l \gg \Delta$. The subfilter-scale (SFS) turbulence closures are generally of the same form for the two modelling approaches, following a scalar eddy-diffusivity (K) model, like $K \propto E^{1/2} l^s$, where E is the turbulent kinetic energy, the difference laying in the length scale, respectively l and Δ . In coarse-resolution mesoscale modelling the turbulent fluxes are entirely carried by the SFS model, while in high-resolution LES the SFS model has the principal role of extracting energy and scalar variance from the filtered scale. However, when $l \approx \Delta$, here defined as ‘*terra incognita*’, like for very high resolution mesoscale modelling, the SFS model “(...) carries appreciable flux in an environment in which all three components of resolved

gradients can be significant". Wyngaard showed that the SFS model consistent with SFS flux conservation equations has a tensor diffusivity and that the tensor nature of the diffusivity can be important in modelling the *'terra incognita'*.

1.3 Initialization and input data

Meteorological, surface data and observations that can be used as input for initialization and nudging in the mesoscale model, are often provided at resolution lower than 1 km. However, in principle to build an effective driving information on a 1-km-resolution computational grid, it is desirable to have input data available at a higher resolution.

Often, the data available by default for input to mesoscale models, such as digital elevation model (DEM) for topography, like the GTOPO30 (30") USGS, and land-use/land-cover data, are instead still limited to 1-km resolution, and relatively old databases are used because they are promptly-ready. Therefore, it is desirable for the modeller or model-user, to include more modern datasets, among them for instance the satellite-based data. These are available for many surface parameters, such as land use, vegetation fraction, albedo, snow cover and soil moisture. Most of the satellite datasets are released with resolutions of 500 or 1000 m, still maybe too coarse for 1-km grid-cell simulations but yet better than the outdated surface parameters in the default datasets. In particular, for high-resolution regional and local-scale simulations in complex terrain, an accurate representation of the topography and surface properties is very important. When performing model simulations, the topographic features are smoothed by the procedures interpolating the input data on the grid points at the model resolution, leading to mountain peaks that are lower and valley floors that are more elevated than in reality. It is clear that having DEM data with a resolution (much) higher than the model one may improve the accuracy in the description of the topography, while rough input data deteriorate it.

The importance of the orographic input and the effect of its interpolation procedures will be treated in next Section 2. Here we consider another fundamental aspect for the initialization and driving of the model simulations, that is the initialization of soil variables. Soil moisture and temperature change in time and they strongly influence the surface fluxes, the interaction between the atmosphere and the surface and thus the local dynamics. Generally, the standard data used for initialization are available at coarse resolution, such as from global models outputs or from sparse measurements, and are characterized by a high uncertainty. Inappropriate initial values of these variables may largely affect the performance of the model simulations, not only at the surface but also in all the atmospheric boundary layer. In addition, as noticed in Arnold et al. (2012), in complex terrain *"the effects of the real land-use and features associated with topography (such as cold air pools in valleys and basins during the cold season) are not properly represented"*.

In the frame of the preliminary simulations performed for the Frejus transect case study, in a set of runs we have included the town of Turin and part of its surrounding plain the smallest domain. In Figure 1.11, the domains covered with the related Grids 3 and 4 are showed. The 3D configuration of the grids 3 and 4 of RAMS-MIRS models is respectively 196 x 132 x 17 km with an horizontal grid mesh of 4 x 4 km, and 133 x 61 x 17 km for the with a grid mesh of 1x 1 km.

In Figure 1.12, we compare the wind-speed simulations against observations at Torino-Consolata station, located in the centre of Turin. We consider this station as a reference since it provides measured data of high quality and it is fully representative of the urban characteristics. It represents a severe test for the reliability of the model simulations, since the city is identified at the regional scale mainly through its land use and roughness, while of course the urban scale is not resolved. When the model is able to capture, on average, the mean variables at such kind of stations, then we can be confident in its good performances in less critical part of the domain. For instance, the relatively good agreement of the measured

wind speed with predicted values at the four grid points around the station supports the application of the modelling system at this resolution. Analogous results are found also at high-mountain stations, like Bardonecchia (Figure 1.12) and Modane, which are the two villages hosting the entrances of the Frejus tunnel, both in the Summer (July) and in the Winter (December and February) episodes.

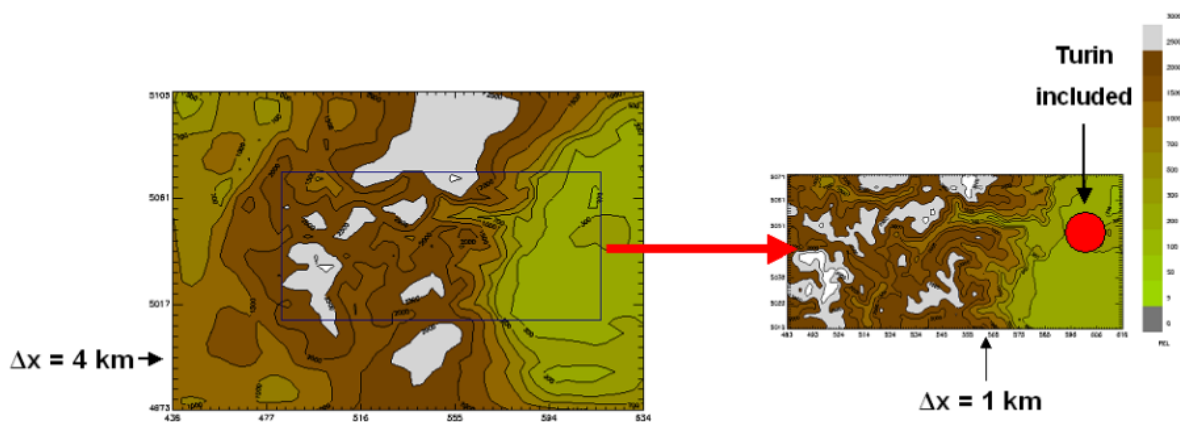


Fig. 1.11: Grids 3 and 4 for the Frejus preliminary simulations.

These preliminary runs are useful to highlight the problem related to the modelling of the surface temperature in highly complex terrain, which occurs especially when simulating the meteorology in winter time. In fact, the mesoscale models, and in our case RAMS, need an initial profile of temperature and humidity in the soil. These profiles represent the triggering-start of the soil model, which is part of the 'engine' of the surface layer and boundary layer physical processes.

As anticipated above, the international community of modellers and meteorologists recognised that the lack of observed data and information about the soil thermodynamical variables is one of the limits that can affect the performances of the numerical models. This problem becomes even more 'dramatic' for simulations of winter periods, since also the quality of information about the snow coverage is not yet optimal.

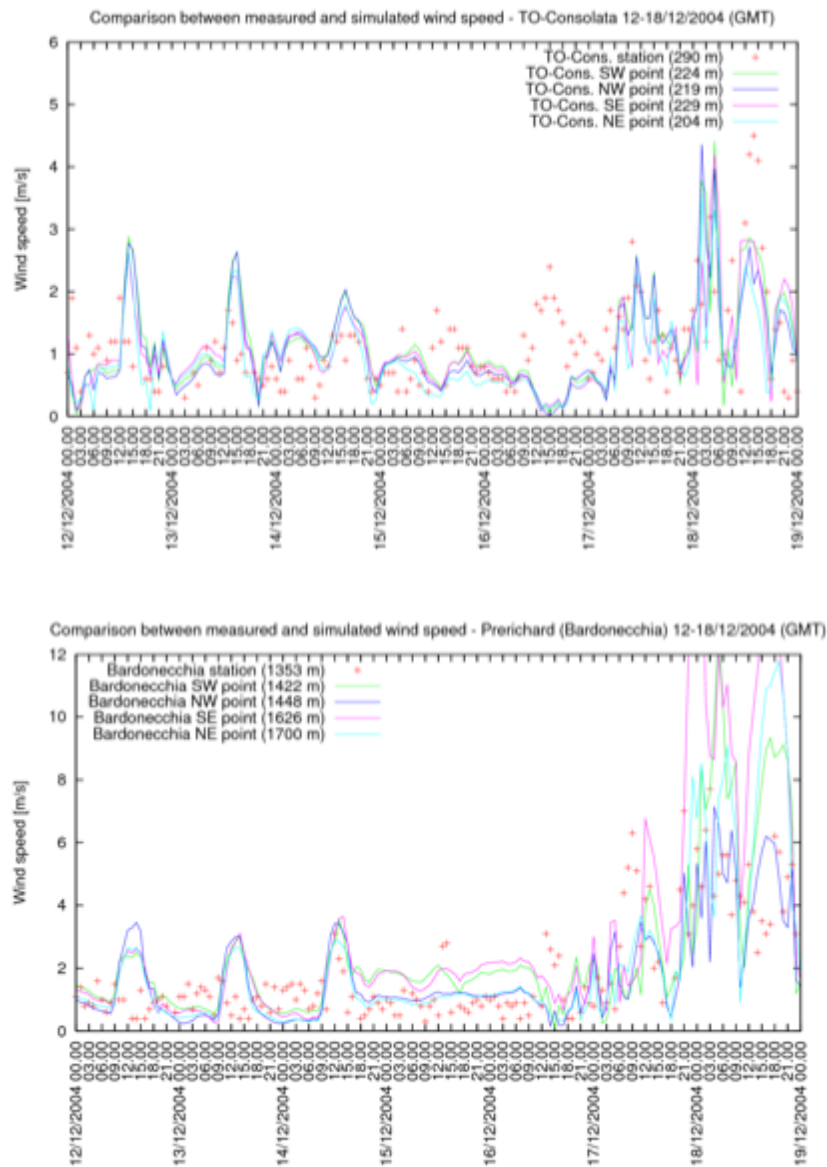


Fig. 1.12: Simulation in December. Comparison between wind speeds measured and simulated in Torino-Consolata station (top) and Bardonecchia station (bottom).

In these preliminary simulations, we adopted as initial soil profiles of temperature and humidity the values extracted by the ECMWF analyses, which of course are provided with a resolution of 0.5 degree (that is, at our latitudes, about 50 km). In Figure 1.13, we present the temperature trend at Bardonecchia in the episodes of July and December. While in July the agreement is satisfactory, in December a very large difference between predictions and observations is obtained. This was one of the worst cases, but it is representative of the problem. We notice that the model is hardly able to become independent from the initial conditions, and only after 1 day of run start-up and 5 days of simulation the predicted temperature start to match the measured value. In the first days, the daily cycle is not correctly reproduced and, in particular, the minimum values are not captured at all. This deficiency does not occur in the July episode, where the same one-day run start-up time was used.

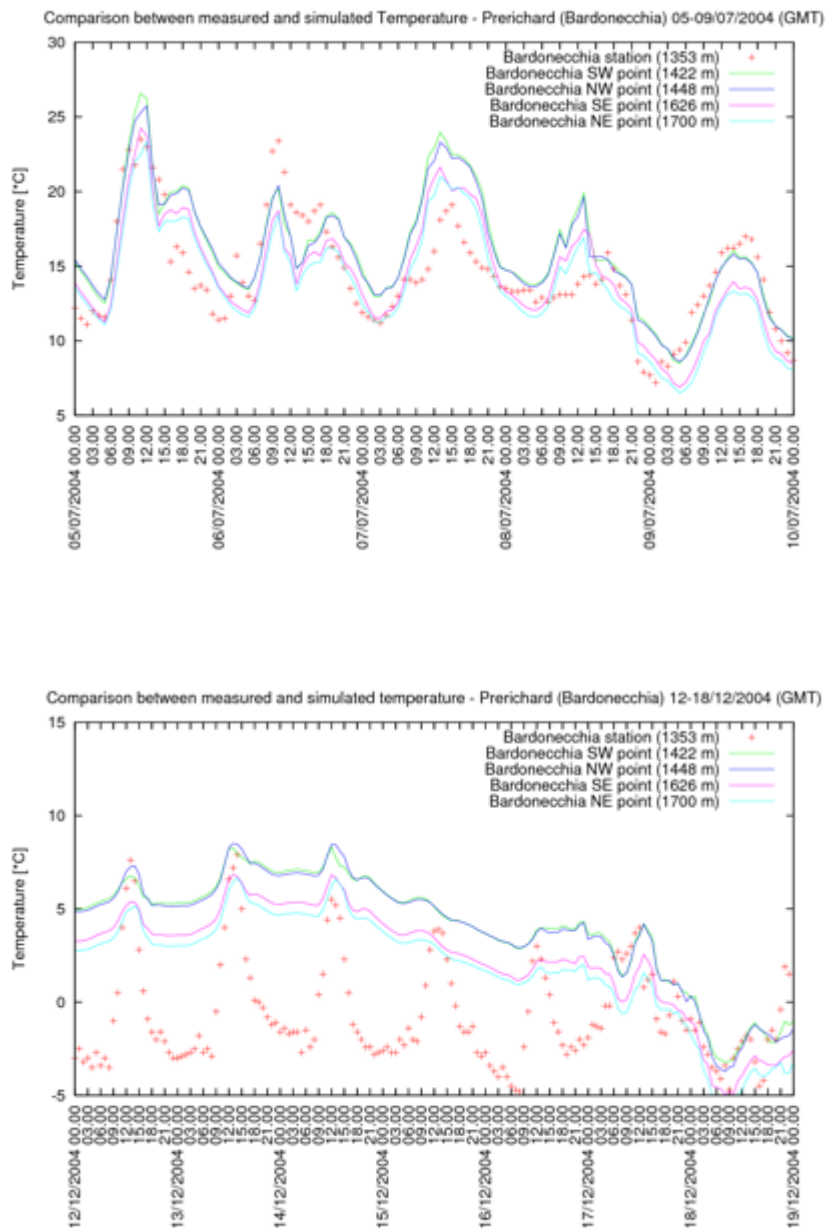


Fig. 1.13. Comparisons between temperatures measured and simulated in the Bardonecchia (Prerichard) for the summer-July (top) and winter-December (bottom) periods in the preliminary simulations.

To overcome this inaccuracy, we varied the initial profiles of soil temperature and humidity on the basis of our previous experiences and of discussion within the community of RAMS modellers.

We found out that using a constant profile of humidity with lower values than the ECMWF ones improves the performances of the model, due to a better budget of the soil-air fluxes in the soil model. An example is given for the results of the set of simulations corresponding to the domains of Figure 1.1. For the sensitivity runs, a constant value of relative humidity was used for the humidity profile in the soil. Results are shown for a value of $RH = 0.25$ in Figure 1.14 for the critical episode of December.

Improvements in the daily cycle and in the temperature range are obtained, even if the deficiency is not completely overcome. In some of the other stations, like Mont Cenis, the improvement in the December episode simulation was larger. On the other hand, simulating

the other winter episode of February with the same configuration gave satisfactory results also with the ECMWF profile. We notice that the quality of the reproduction of the wind velocity field was anyway unaffected by the changes in the initial soil profiles.

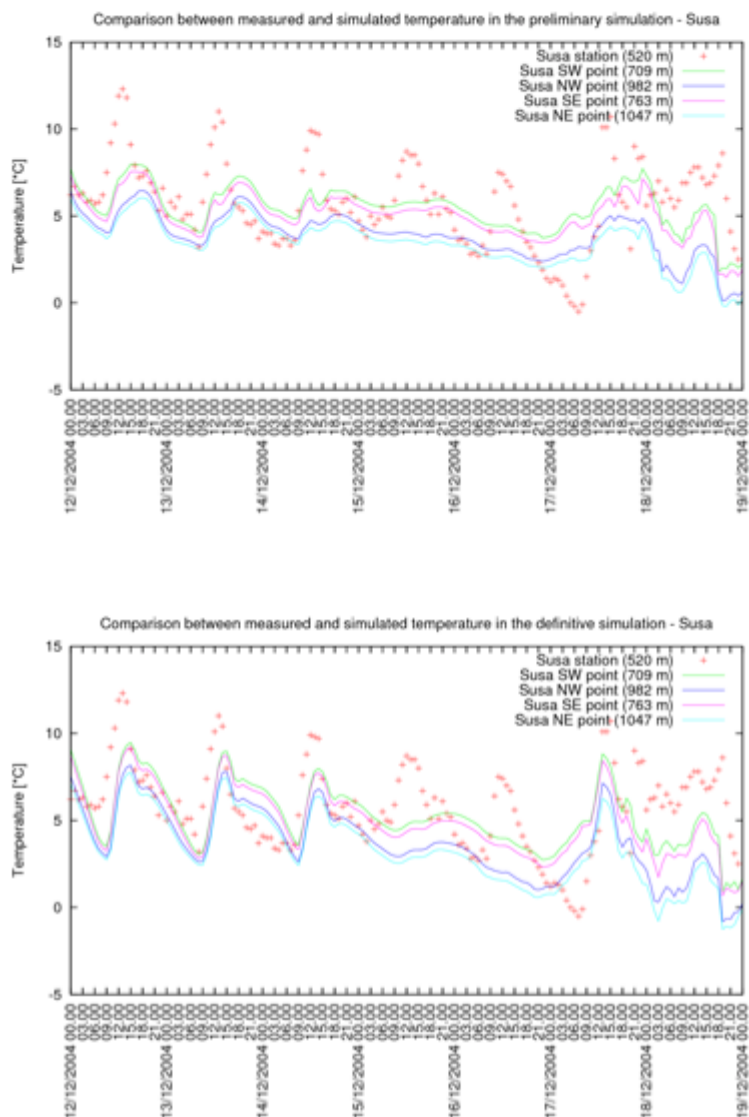


Fig. 1.14. Comparison between temperatures measured and simulated using the ECMWF soil humidity profile (top) or a constant value of RH=0.25 (bottom) simulations in Susa.

Another approach could be to produce mesoscale simulations on a single coarse grid for a long period, at least one month, and then use its final output values of the soil thermo-fields as input to the simulation of episodes. This approach would help overcome the problem of the initial-condition dependency in time, but of course is computationally expensive and needs further tests.

It is also possible to use an off-line hydrological model jointly with available soil moisture measurements, to produce high-resolution soil moisture fields for the domain.

When considering data assimilation from surface station, for high resolution simulations a high density of measuring stations is required, but this requirement is hardly achievable, more frequently for case studies accompanied by dedicated field campaigns. In complex terrain, the problem of the representativeness of the observations remains: even if high-density data are available, they might be not representative of the variability of the topography and their use might also affect negatively the performance of the model. This

aspect influences also the use of off-line soil models, since they require gridded input data elaborated from observations, which, again, in complex terrain are generally inadequate to properly represent the variability of the topography.

Regarding the possible use of satellite-based remote sensing data, in Wagner et al. (2012) it was found that they are not be able to account for the variability in complex terrain. In any case, to obtain performing simulations it is important to use input information, such as soil moisture, vegetation coverage, snow cover and albedo, that is more accurate than the standard information provided with the models, also to account for their variability not only in space but also in time, as a function of the season and in response to the meteorological changes themselves. In this context, the use of the time-dependent information that is provided by the satellite products should be evaluated.

1.4 Computational and numerical issues

As discussed in the Introduction, several studies demonstrated that in complex topography using high resolution, of the order of 1 km or less, allows capturing terrain-induced atmospheric processes that would be poorly represented at lower resolutions. The agreement with the observations largely improves already passing from 3-4 km to 1 km resolution.

A shortcoming of high-resolution runs lays in the consequent high computational costs. For example, a transition from 9 to 3 km resolution would result in a 9-fold increase in number of horizontal grid points and a 3-fold increase in the number of time steps. This imply that a 9-km resolution run taking one hour would take about one day at 3-km resolution and up to even one month at 1 km (Arnold et al., 2012). In addition, a problem of data storage may originate, given that the output files result to be much bigger for higher resolution runs.

This kind of problems, included also the post-processing procedures, are affordable using parallelization techniques for numerical computing.

Considering numerical issues, in complex terrain for high resolution two main aspects have to be accounted for, the choice of the discretization scheme and the problem related to the vertical coordinate system.

The performance of the mesoscale atmospheric models is highly dependent on the scheme used, generally based on finite-difference discretization methods and explicit or semi-implicit time integration. These have to be chosen regarding their accuracy, stability, and impacts of implicit and explicit diffusion and computational cost. Generally, sensitivity tests are needed when applying the models to very complex orography for simulation where the spatial and temporal resolution is high. Numerical noise in complex terrain may be enhanced due to the forcing of the steep orography, which is a challenging condition for the advection scheme and the pressure-gradient discretization. Smoothing or filtering the orography is done to control such problems, but at the same time, this can compromise the proper representation of the topography and the effectiveness of the high resolution approach.

Specific studies are dedicated to investigate the applicability in models of alternative discretization schemes, such as finite-volume, immersed-boundary method and finite element. Regarding the coordinate system, generally terrain-following coordinates are used, in pressure or height. These might be problematic in very complex orography and high resolution and true Cartesian coordinates can become a better alternative (Walko and Tremback, 2002). Other computational and numerical aspects concern the sensitivity to the spin-up time and the possible divergence of the simulation for very long run periods. All these aspects are treated in literature: in next Section, we present some results related to tests performed with RAMS on these items.

2. Preliminary RAMS simulations in the HKKH area

In the frame of RAMS modelling activities, it was planned to perform high-resolution (cloud-resolving) simulations for specific complex topography areas to investigate relevant physical and dynamical processes over the mountainous areas of the Hindu Kush-Karakorum-Himalaya (HKKH). The results could be evaluated using available observations and will be released to the NextData archives.

In the first phase of RAMS modelling activities, a thorough review of the specialized literature on high-resolution simulations in highly complex terrain has been conducted as detailed in previous chapter. This allowed identifying the critical aspects of performing simulation of the atmospheric circulation in very inhomogeneous topographical conditions. Then, thanks to the analysis of RAMS simulations performed in the Italian Alps, specifically in the Frejus areas, some guidelines were established for the sensitivity analysis to carry on with RAMS simulations in the HKKH case study, where a further thorough analysis of critical issues related to the simulation of physical processes in very complex orographic settings has been attained through high-resolution simulations. Here we present details and examples of simulations performed in the HKKH area, focusing on their sensitivity to grid resolution, orography representation, level of the microphysics parameterization, and to some numerical aspects. The latest RAMS version 6.0 has been used for the simulations. To read the output meteorological variables we used the RAMS post-processing package REVU (RAMS Evaluation and Visualization Utilities). REVU is the standard supported package for generating graphical representations and reformatting RAMS model output. REVU's function is to read "analysis" files written from a RAMS simulation, select user-specified fields and cross sections from the file data, and plot the field cross sections, or output the selected data in one of several available formats (e.g. Vis5D, GrADS, GRAB, DUMP). REVU can also interpolate point data from the analysis files.

2.1 Description of the case study and of the model runs

We chose a reference case characterized by a flood event that was previously studied. An unexpected heavy rain and a flood occurred in Pakistan during the week 24-31/07/2010. This unusual episode has been studied and linked with other critical events, for example heat waves in Russia.

In the RAMS model, the two-way grid nesting interactive procedure provides a 'zoom' from large-scale area to smaller scale domains, and the non-hydrostatic option allows representing all meteorologically relevant spatial scales. In particular, the two-way nesting procedure allows optimising the interaction between the different scales. The simulations were thus configured using four nested grids with a horizontal grid resolution of 64 km, 16 km, 4 km and 1 km, respectively: the main outer one covers a wide domain, where the main large scales topographical features of the HKKH region are included. The next two intermediate grids zoom over the area of interest and they are chosen to be compatible with the main local topographic features. The last domain, having the highest resolution, is focused over the HKKH area where the observation stations were selected for the NextData Project. The 3D configuration of the four grids is described in Table 2.1.

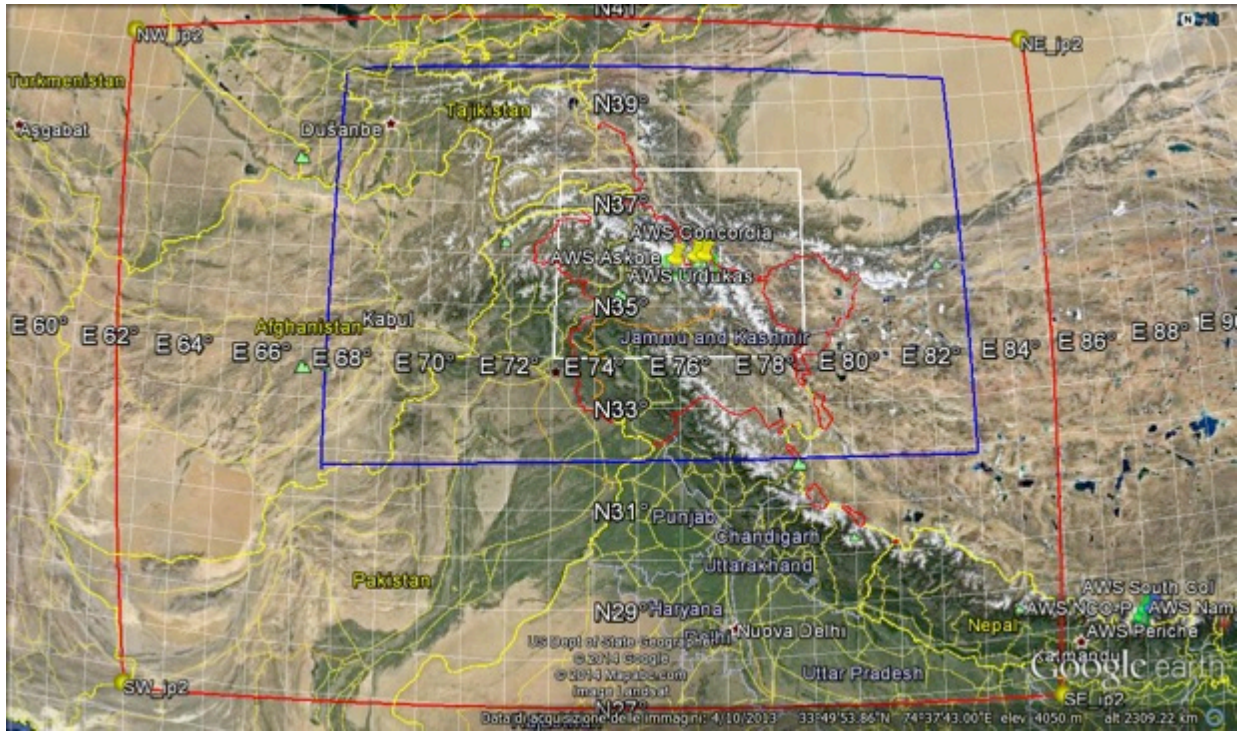


Fig. 2.1. Simulation domains (four nested grids) with the NextData stations (code number: 8-10) in yellow.

	GRID1	GRID2	GRID3	GRID4
Horizontal dimensions (km)	2112 x 1728	1488 x 912	340 x 228	105 x 45
Horizontal grid resolution (km)	64 x 64	16 x 16	4 x 4	1 x 1
Number of vertical levels	27	27	27	27
Top of the domain (km)	19251.3	19251.3	19251.3	19251.3
Number of x gridpoints (W-E)	34	94	86	106
Number of y gridpoints (N-S)	28	58	58	46
Center latitude (°dec)	34	36.2905	36.1425	35.7961
Center longitude (°dec)	74	75.7856	76.0497	76.3071
SW point (LAT,LON) (°dec)	(25.803, 63.506)	(32.045, 67.802)	(35.134, 74.154)	(35.603, 75.721)
NE point (LAT,LON) (°dec)	(41.126, 86.573)	(39.948, 84.586)	(37.120, 77.992)	(35.986, 76.896)

Tab. 2.1. Four grids 3D configurations used in RAMS.

The modelling activities are focused on the Central Karakorum National Park (on Baltoro Glacier). In this region, three Automatic Weather Stations are installed. We also considered seven stations of the Pakistan Meteorological Department (PMD). For each station, we summarized the main characteristics in Table 2.2.

CODE	NAME	LON (°E)	LAT (°N)	ALTITUDE (m)	GRIDS
8	Askole	75.815	35.681	3015	1,2,3,4
9	Urdukas	76.286	35.728	3926	1,2,3,4
10	Concordia	76.514	35.744	4700	1,2,3,4
14	Astore	74.9	35.33	2168	1,2,3
15	Skardu	75.68	35.30	2317	1,2,3
16	Gupis	73.40	36.17	2156	1,2
17	Chitral	71.83	35.85	1498	1,2
18	Gilgit	74.33	35.92	1460	1,2,3
19	Bunji	74.63	35.67	1372	1,2,3
20	Chilas	74.10	35.42	1250	1,2

Tab. 2.2 Coordinates of the measuring stations in HKKH area: NEXTDATA stations (code number: 8-10) and PMD stations (code-number: 14-20).

The initialisation of the RAMS model is obtained from the (ECMWF) analyses with a resolution of 0.5 degree (that is, at our latitudes, about 50 km). In input to RAMS, the large-scale 3D meteorological fields give the initial conditions and the boundary conditions that drive the model during the simulation by means of the nudging technique.

In the selected period, we performed simulations for two cases, named as follows:

- “one-day case”: 21/07/2010
- “one-week case”: 24-31/07/2010

The “one-day case” run.

A one-day (21/07/2010) case study has been carried out in order to perform some tests on the sensitivity to the smoothing of topography.

In RAMS, the flag ITOPSFLG controls the type of processing of topographic data from input files. This is a 3-step process that involves topography information being defined successively on 4 different grids, called as the ‘O’, ‘P’, ‘Q’, and ‘R’ grids. First, a horizontal interpolation is carried out in order to transfer data from the ‘observed’ or O grid of the input file, to a polar stereographic grid of comparable resolution, which is the P grid. The P grid uses the same projection as the RAMS grid (the R grid) where the data will reside in its final state, but is usually of much higher resolution. Second, data is averaged from this P grid to a lower-resolution Q grid, which is also polar stereographic and has a horizontal grid spacing that is an integer multiple of that on the P grid. This step automatically filters out small scale variations which are not desired on the model grid. In this second averaging step, a choice of averaging algorithms exists and ITOPSFLG is the flag that selects choice to be used.

There are four topography options:

- *Average Orography*: a conventional mean is computed where terrain heights for all P grid cells in a single Q grid cell are summed and divided by that number of P values, to obtain the value for that Q cell (ITOPSFLG = 0).
- *Silhouette Orography*: both the conventional mean and a silhouette average are computed, and the value assigned to the Q grid cell is a weighted average of these. The silhouette average finds the mean height of the silhouette, as viewed from the east or west, of the set of P grid terrain heights contained within a single Q grid cell, and a separate silhouette height as viewed from the north or south and averages the two silhouette heights together. This becomes the computed silhouette height for that

coarse-grid cell. While the conventional average preserves total terrain volume above sea level, the silhouette average adds mass by filling in valleys. It is used to maintain the effective mean barrier height that air must rise to when crossing a topographic barrier such as a ridge. The conventional average lowers this barrier height, particularly when the barrier height is poorly resolved (ITOPSFLG = 1).

- *Envelope Orography*: an envelope topography scheme is used to obtain Q grid values from P grid values. It is an alternative method of attempting to preserve barrier heights (ITOPSFLG = 2).
- *Reflected Envelope Orography*: a reflected envelope topography scheme is used and it aims at preserving both barrier heights and valley depths. Naturally, this method leads to the steepest topography in RAMS, while still filtering the shortest wavelengths. In the third and final step, topography is interpolated from the Q grid to the R grid, and the R grid is usually of moderately higher resolution than the Q grid (ITOPSFLG = 3).

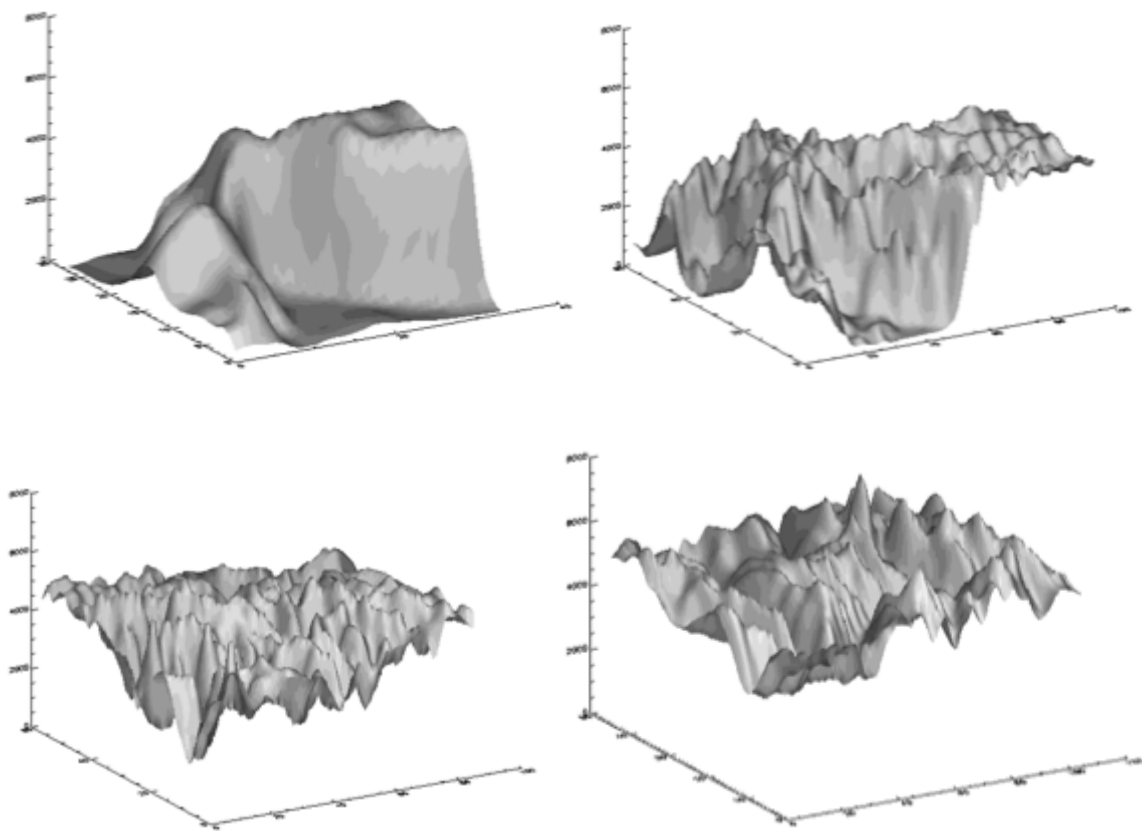


Fig. 2.2. Surface plot of the orography for ‘Reflected Envelope’ option at the four grids. Grid 1, top left; grid 2, top right, grid 3, bottom left, grid 4, bottom right.

We analysed the resulting topography for all cases. In Figure 2.2 the orography as resolved on the four nested grids for the option with the Reflected Envelope Orography is plotted as an example.

In Figure 2.3, we report the contours of the differences between the orography for two cases, computed at each grid point as the values from Reflected Envelope Orography minus the values of the Average Orography, in the four grids. Contours are plotted for a range between -400 to +400 m every 50-m difference. The largest differences negative/positive in all domains are -155.04 and 329.99 m in Grid 1, -389.54 and 337.20 m in Grid 2, -241.37 and 354.08 m in Grid 3, -94.10 and 205.35 m in Grid 4. In all cases, they might affect the simulation of the local characteristics of the flow in a non-negligible way.

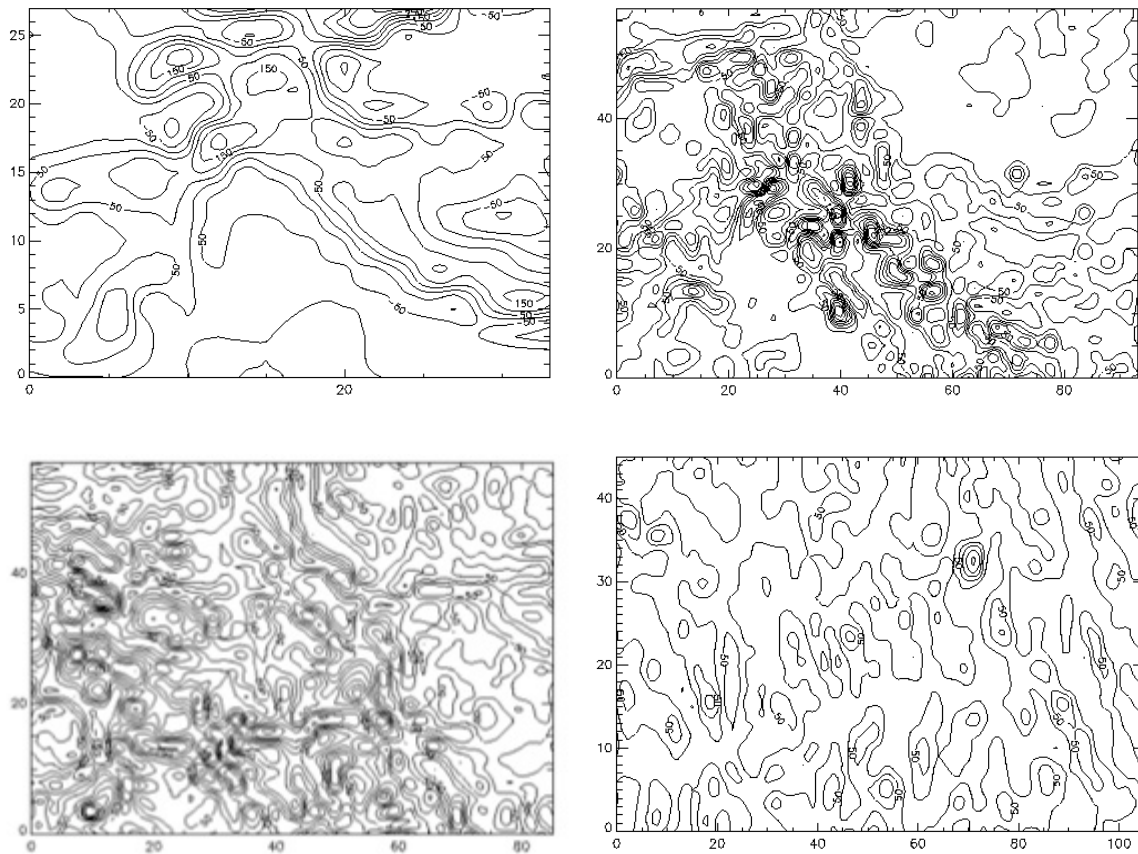


Fig. 2.3. Contours of the differences between the orography values for ‘Reflected Envelope’ and ‘Average’ options. Grid 1, top left; grid 2, top right, grid 3, bottom left, grid 4, bottom right.

An estimate of the effect that these differences induce on the meteorological variables was obtained completing two simulations, the first with the “smooth” *Average* option (ITOPSFLG=0, Case_top0) and the second with the more “complex” *Reflected Envelope* option (ITOPSFLG=3, Case_top3). The obtained results are used for the intercomparison exercise between simulations dealing with different scheme of orography.

To extract the variables at single stations or points in the four domains, we used the option “GRAB” which reads in input the lat-lon coordinates of the station and then it transforms them in metric coordinates, which are afterwards transformed in latitude and longitude again. By means of this method, we verified that in the last step the station coordinates are a bit different with respect to the real ones, supplied in input, and as a consequence also the station altitude changes. In particular, in complex terrain, this effect is emphasized and the change in altitude has to be clearly taken into account.

We note that for all NextData stations, we found different altitudes in the four grids using REVU option “GRAB”, due to the different adjustments of the geographical coordinates:

Askole (3000 m): grid 1: 4351 m; grid 2: 4380 m; grid 3: 4465 m; grid 4: 3431 m

Urdukas (3926 m): grid 1: 5155 m; grid 2: 5400 m; grid 3: 4400 m; grid 4: 4113 m

Concordia (4700 m): grid 1: 5051 m; grid 2: 5248 m; grid 3: 4974 m; grid 4: 4579 m

In this qualitative evaluation, where we make comparisons of predicted outputs at the same grid point for the four domains, such differences are not important. They would instead affect a comparison with observed data. For this reason, when simulations are compared to observations, as previously done we consider the four grid points around the station, in order to have a glance on the variability in the predicted meteorological variables associated to the topographical complexity of the region.

Hereafter we report the simulated results of the two simulations, Case_top0 and Case_top3, at the three NextData stations (n. 8-9-10) for temperature and wind speed. In particular, we computed the difference in the temperature and wind speed values, respectively, as

$$\Delta T = T_{\text{Case}_{\text{top}0}} - T_{\text{Case}_{\text{top}3}} \quad \text{and} \quad \Delta U = U_{\text{Case}_{\text{top}0}} - U_{\text{Case}_{\text{top}3}}.$$

In Figure 2.4, regarding the two different orography schemes, we plot the temporal trend of the temperature and wind-speed differences, ΔT and ΔU , for each grid. The differences between temperature values are less enhanced in grids 1 and 2, where the values have been extracted at comparable altitudes, than in grids 3 and 4. In grid 3, ΔT is almost nearly positive, therefore $T_{\text{Case}_{\text{top}0}} > T_{\text{Case}_{\text{top}3}}$. In grid 4, the trend is different: ΔT is negative for about 18 hours and then it becomes positive $T_{\text{Case}_{\text{top}0}} > T_{\text{Case}_{\text{top}3}}$. The differences in wind speed varies depending on the station and they are generally more enhanced in the finer grids 3 and 4. Major drifts between the two runs occur during daytime, where the difference in slopes and peaks due to the smoothing can play a fundamental role on the radiative effects and the consequent heating of the surfaces, affecting thus both the temperature field, the circulation in the valley, the mountain-valley flow and breeze.

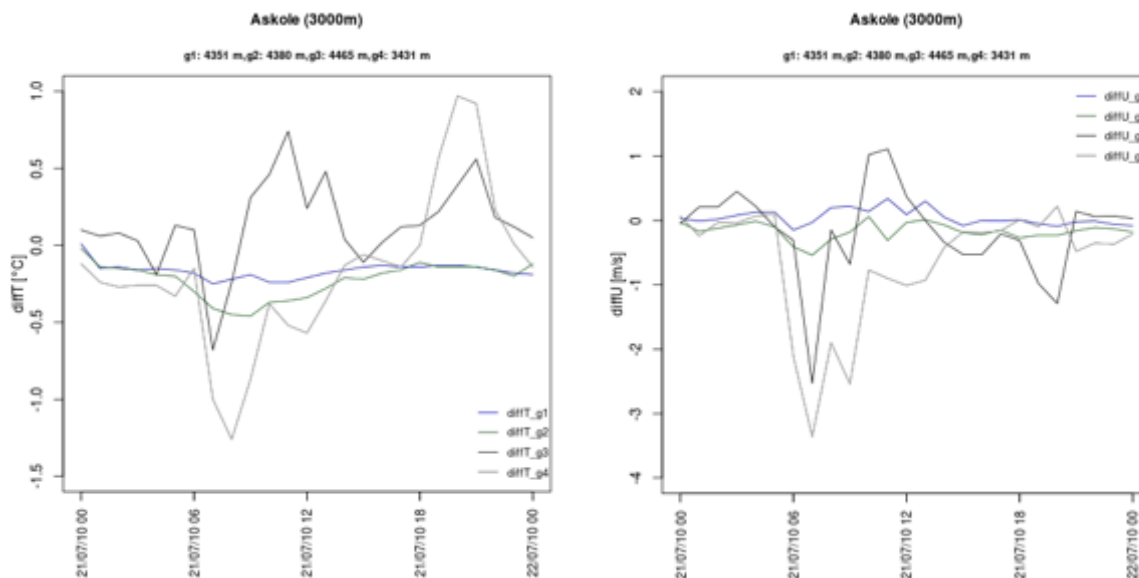


Figure 2.4. (continues...)

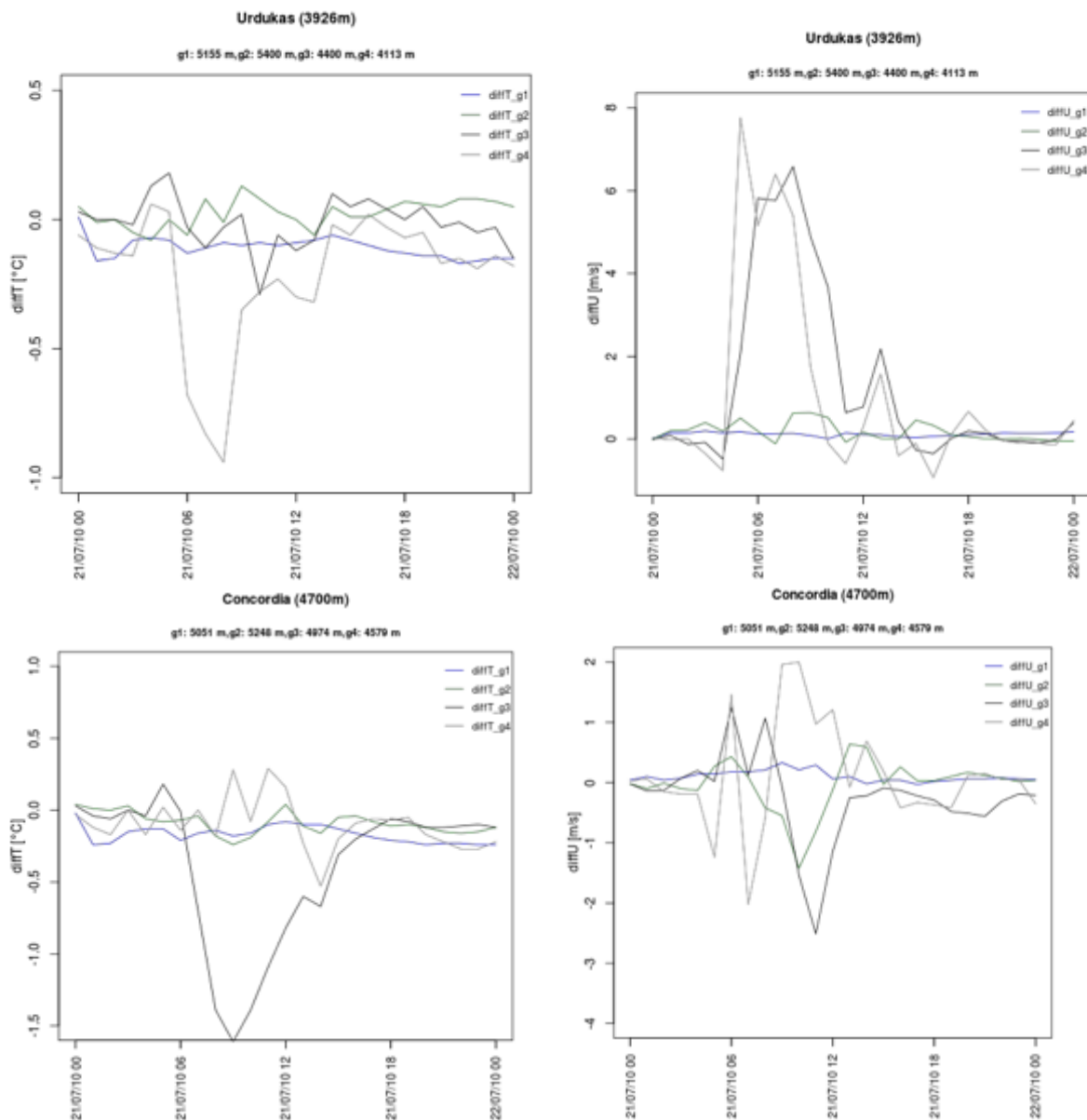


Fig. 2.4. One-day case study. Comparison between the difference in temperature ΔT (left) and wind speed ΔU (right) for Case_top0 and Case_top3 runs, in the four grids at NextData Askole (top), Urdukas (centre) and Concordia (bottom) stations, respectively.

As an additional analysis, in Figure 2.5 the relative humidity daily trend is plotted at the Askole and Concordia stations for the two orography smoothing options. Again, larger differences occur in the finer grids 3 and 4, mostly in the central hours of the day.

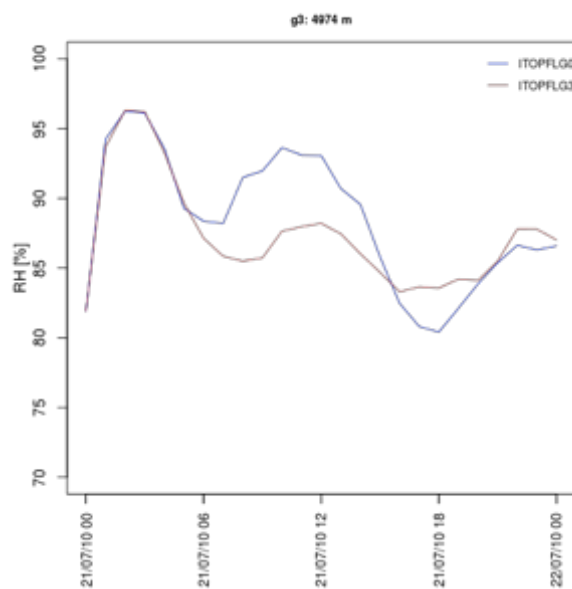
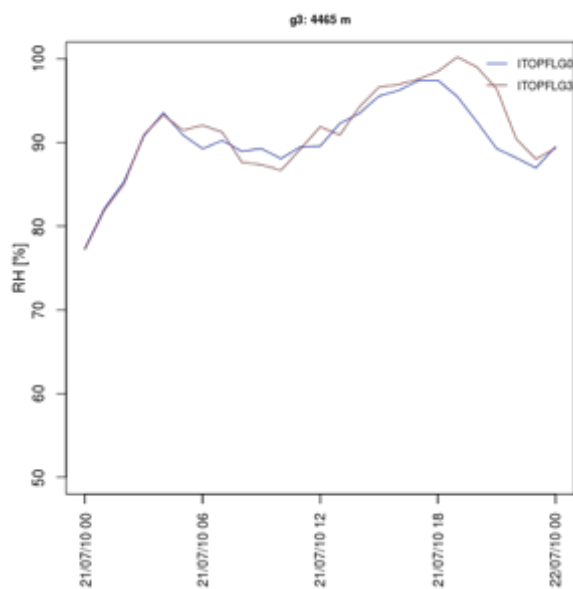
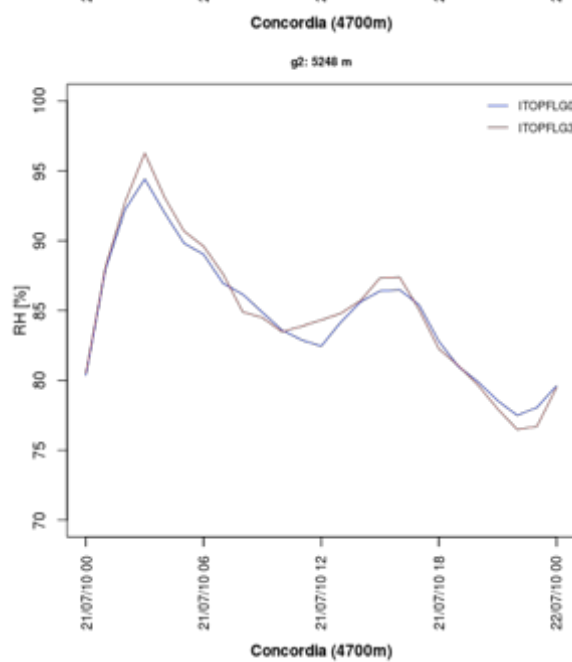
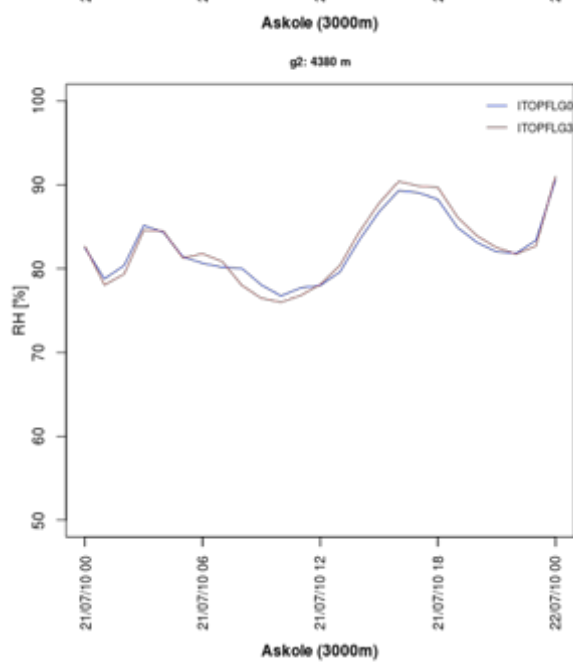
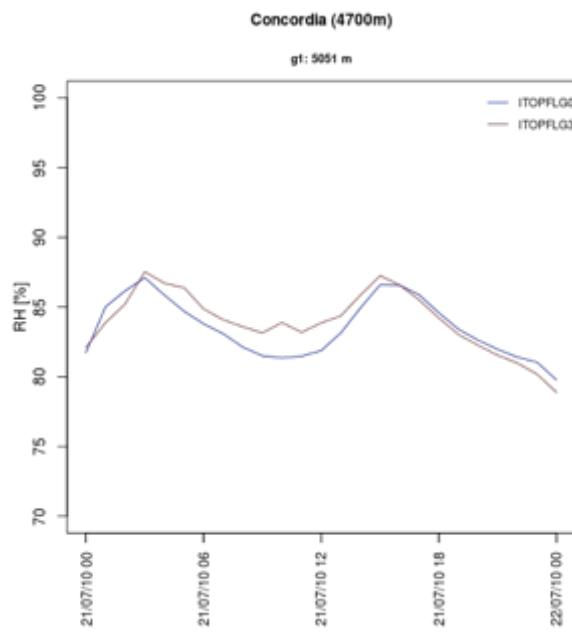
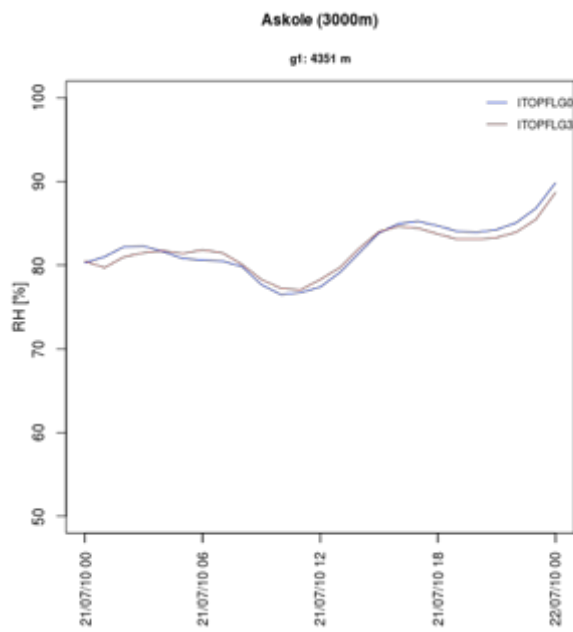


Figure 2.5. continues...

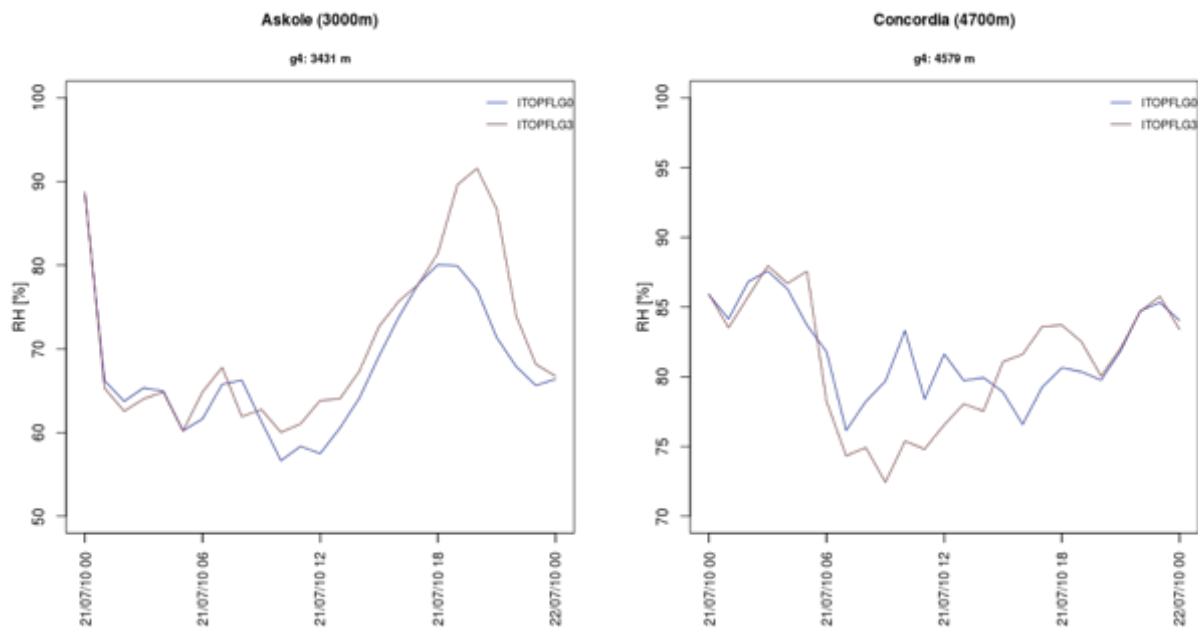


Fig. 2.5. One-day case study. Comparison between the relative humidity for Case_top0 and Case_top3 runs, in the four grids at NextData Askole (left) and Concordia (right) stations, respectively.

To have an overall estimate of the differences in the meteorological variables induced by different way of smoothing the orography, in Figure 2.6 and 2.7 we present the scatter plots of the predicted values for all grid points of respectively the grids 1 and 4, extracted at the first model level (24 m) at, for instance, 6 a.m.

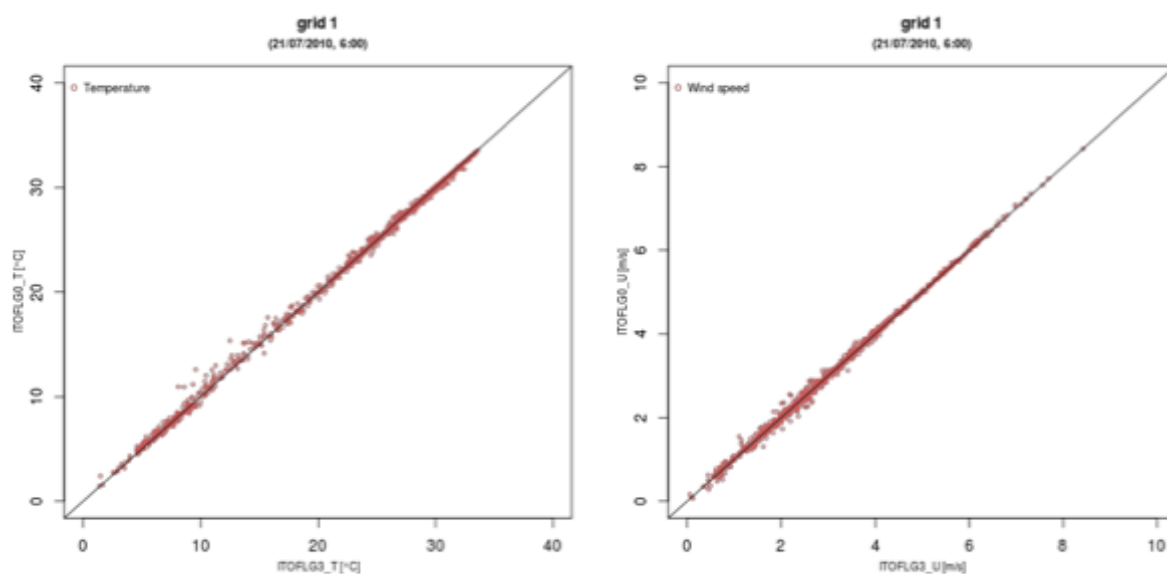


Fig. 2.6. Simulated temperature and wind speed scatter plots for grid 1, using two different orography schemes, Case_top0 (Y axis) and Case_top3 (X axis).

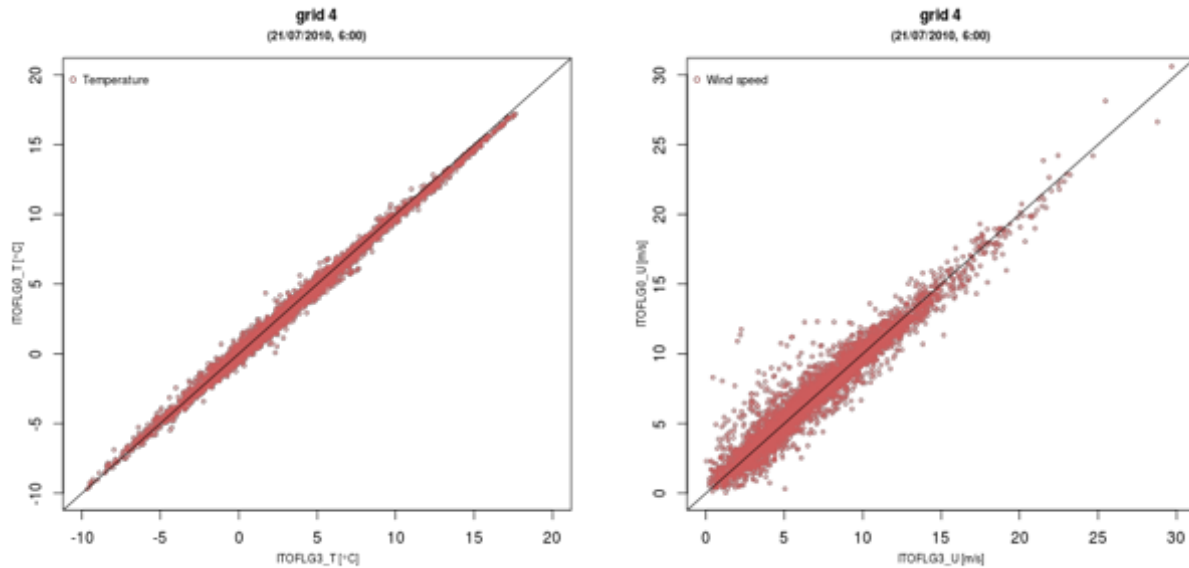


Fig. 2.7. Simulated temperature and wind speed scatter plots for grid 4, using two different orography schemes, Case_top0 (Y axis) and Case_top3 (X axis).

We notice the differences in the ranges of both temperatures and wind speeds in the different grids, linked to the differences in the altitudes. A larger spread between the two sets of wind-speed data is associated to the finest grid, less enhanced for the temperature, when zooming the grid 1 values into the range of the grid 4 ones.

In general, a certain scatter characterizes the temperature data, the largest of the order of $\pm 1^\circ\text{C}$ up to about 10°C occurring in grid 4. Above this temperature value, the simulation with more “complex” orography provides values that are higher than the ones obtained with a smoother orography scheme.

Wind speed values also show substantial differences in the finest grid 4, up to around $\pm 2\text{ m s}^{-1}$ in the lower part of the range.

The analysis shows that the smoothing of the orography has a non-negligible effect on the reproduction of the meteorological fields. When possible, a more realistic representation of the topographical characteristics, which means a lower level of smoothing, should be applied.

The “one-week case” run.

In this case, the RAMS simulation was run for the entire selected period during which the flood occurred, from 24 to 31/07/2010.

In particular, the effect of the microphysics parameterization was investigated.

In RAMS, there are four options for parameterizing the microphysics, determined by the level of their complexity, that is to what extent the moisture and precipitation processes are treated. Hereafter we refer to the different options by the LEVEL flag, as defined in RAMS:

- LEVEL = 0, it causes the model to run dry, completely eliminating any process which influences or is influenced by any phase of moisture. With this option, radiation parameterizations must be turned off.
- LEVEL = 1, it activates advection, diffusion, and surface flux of water, where all water substance in the atmosphere is assumed to occur as vapour even if supersaturation occurs. The value of 1 also activates the buoyancy effect of water vapour in the vertical equation of motion, as well as the radiative effects of water vapour if radiation is activated elsewhere.
- LEVEL = 2, it activates condensation of water vapour to cloud water wherever supersaturation is attained. The partitioning of the total water substance into vapour and cloud water is purely diagnostic in this case. No other forms of liquid or ice water are considered. Both the positive buoyancy effect of water vapour and the liquid water loading of cloud water are included in the vertical equation of motion. Radiative effects of both water vapour and cloud water are activated, if the radiation parameterization is itself activated.
- LEVEL = 3, it activates the bulk microphysics parameterization, which includes cloud water, rain, pristine ice, snow, aggregates, graupel, and hail, or certain subsets of these. This parameterization includes the precipitation process.

In this one-week case study, the “*Reflected Envelope Orography*” topography scheme (ITOP=3) was used and both a complete microphysics parameterization (LEVEL=3), named as TestW_1, and a simplified microphysics parameterization (LEVEL=2), named as TestW_2, were considered.

For the TestW_1 case, we performed and analysed three types of simulation:

- ✓ a complete “continuous” simulation from 24 to 31 July 2010
- ✓ a 36-hours simulation in the same week, in order to test the effect of the spin-up time
- ✓ an “irregular” simulation from 24 to 31 July 2010, during which the RAMS run was virtually interrupted and restarted through the “HISTORY” option, which uses the previously saved output files to carry on the simulation. This was done in order to test the reliability of the restart procedure, which for the initialization uses an analysis state file saved by the model during the run, before the interruption.

The first simulation represents the flood case study; numerical issues have been evaluated by means of the other two cases. In fact, we show that these aspects may influence the model outcome.

Test_W2 case was run as a complete “continuous” simulation, to investigate the effect of the microphysics parameterization when compared to Test_W1 case.

In the following graphs, we report the model results for the period 24-31/07/2010 for two NextData stations, Askole and Concordia. We used an option (DUMP) in the REVU post-processing that supplies as output the fields at the grid points specified in the input file. The simulated fields were extracted from the analysis files at the four grid points around the station, as previously done (SW=South-West, NW=North-West, SE=South-East, NE=North-East).

In Figures 2.8 and 2.9, we show the comparison between the simulated temperature and relative humidity trends, respectively, using the two different microphysics schemes

(TestW_1 and TestW_2 cases) at Askole station. For the comparison we selected the SW point (3841 m) for grid 1 and the SW point (3215 m) for grid 4.

In both graphs of Figure 2.8, we observe that the simulated temperature trends practically superpose until the 28th of July 2010 at 12:00 UTC and then they start differentiating. The values of TestW_2 case (green curve) are higher than those for the TestW_1 case (blue curve) in the last few days. In particular, in grid 4, simulated temperature values for TestW_1 show a different trend compared to the ones calculated for TestW_2. The latter maintains the classic daily temperature cycle: computed values about 15 °C early in the morning and peaks of 20-25 °C at noon. In TestW_1, instead, the model reproduces a perturbation.

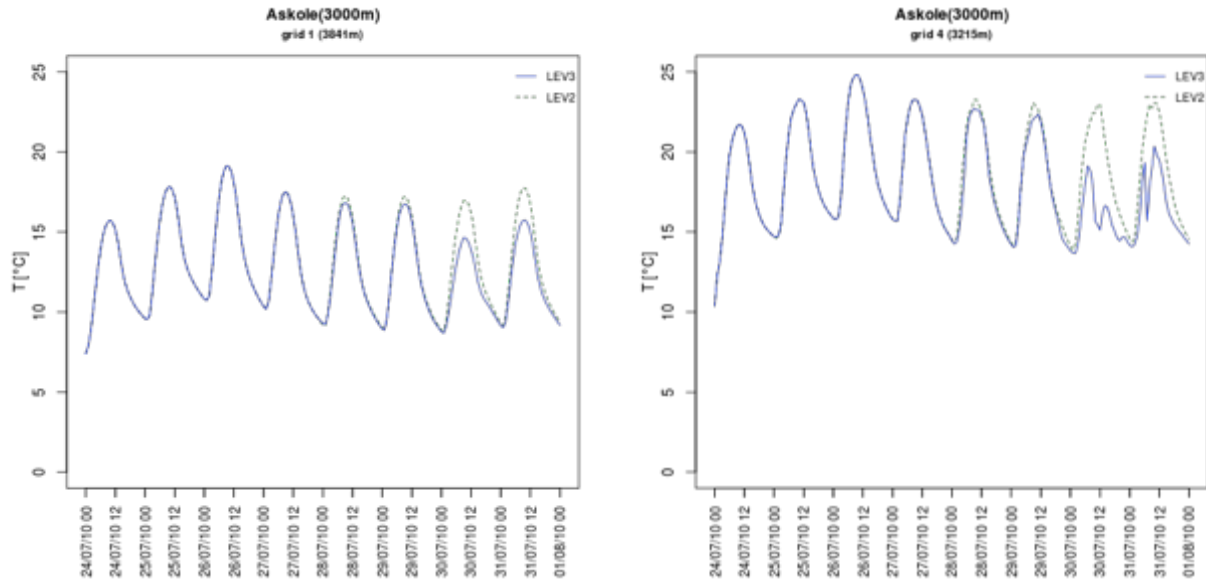


Fig. 2.8. Askole station. Comparison between simulated temperature trends, using two different microphysics parameterization, TestW_1 (blue line) and TestW_2 (green line), at one grid point for grid 1 (left) and for grid 4 (right).

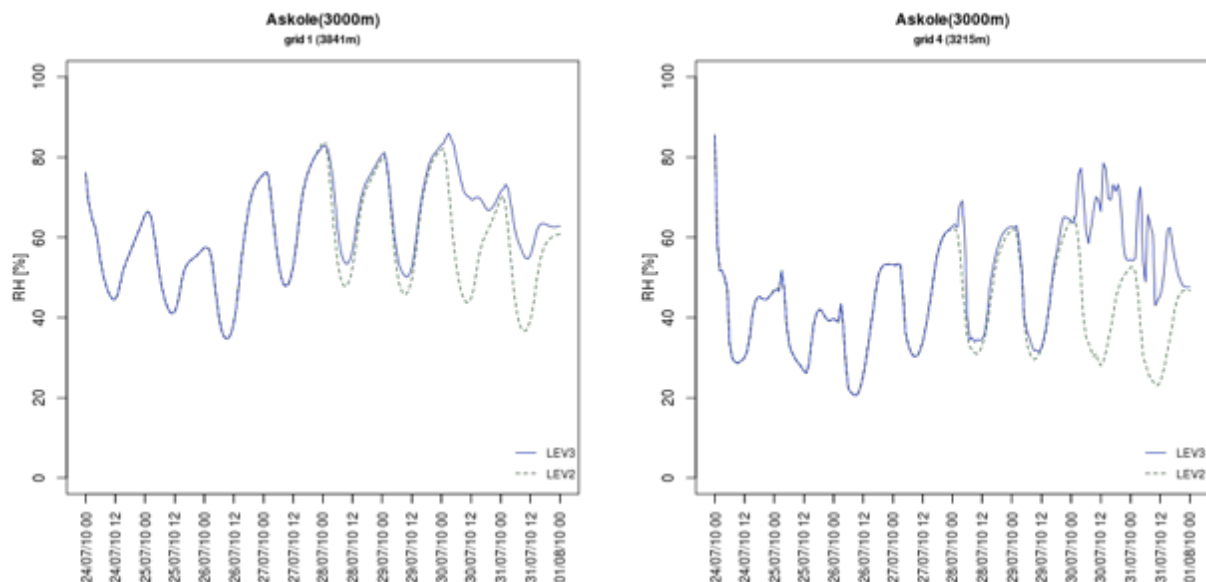


Fig. 2.9. Askole station. Comparison between simulated relative humidity trends, using two different microphysics parameterization, in one grid point for grid 1 (left) and for grid 4 (right).

In Figure 2.9, the simulated relative humidity trends start differentiating especially after the 29th of July at 12:00 UTC. The values of TestW_2 case (green curve) are lower than for the TestW_1 case (blue curve) and in particular simulated relative humidity values for TestW_1 show a different trend compared to the ones calculated for TestW_2. The latter maintains a

cycle in agreement with the temperature. The perturbation found in TestW_1 for the temperature mirrors also in the relative humidity trend.

In Figures from 2.10 to 2.13, we show the same comparison between the simulated temperature and relative humidity trends, respectively, at all four grid points around Concordia station. Here we considered grid 1 and grid 4, to investigate whether the sensitivity to the microphysics schemes shows any trend or is variable.

Like for the previous graphs, we observe that the simulated temperature trends (Figures 2.10 and 2.11) are different, in particular for grid 4, where the simulated values start differentiating just after the simulation begins (on 25th of July 2010 at 0:00 UTC). For grid 4, the differences between the two runs are similar at all four points, while a slightly more variable sensitivity to the microphysics is shown for the nearby points in grid 1.

Regarding relative humidity (Figures 2.12 and 2.13), the sensitivity to the microphysics is enhanced at most points in grid 1 and all points in grid 4. Again, the curves at the four nearby points in grid 4 are very similar thanks to the higher resolution. They may thus be expected to be more representative of the values at the station, when its altitude is not much different.

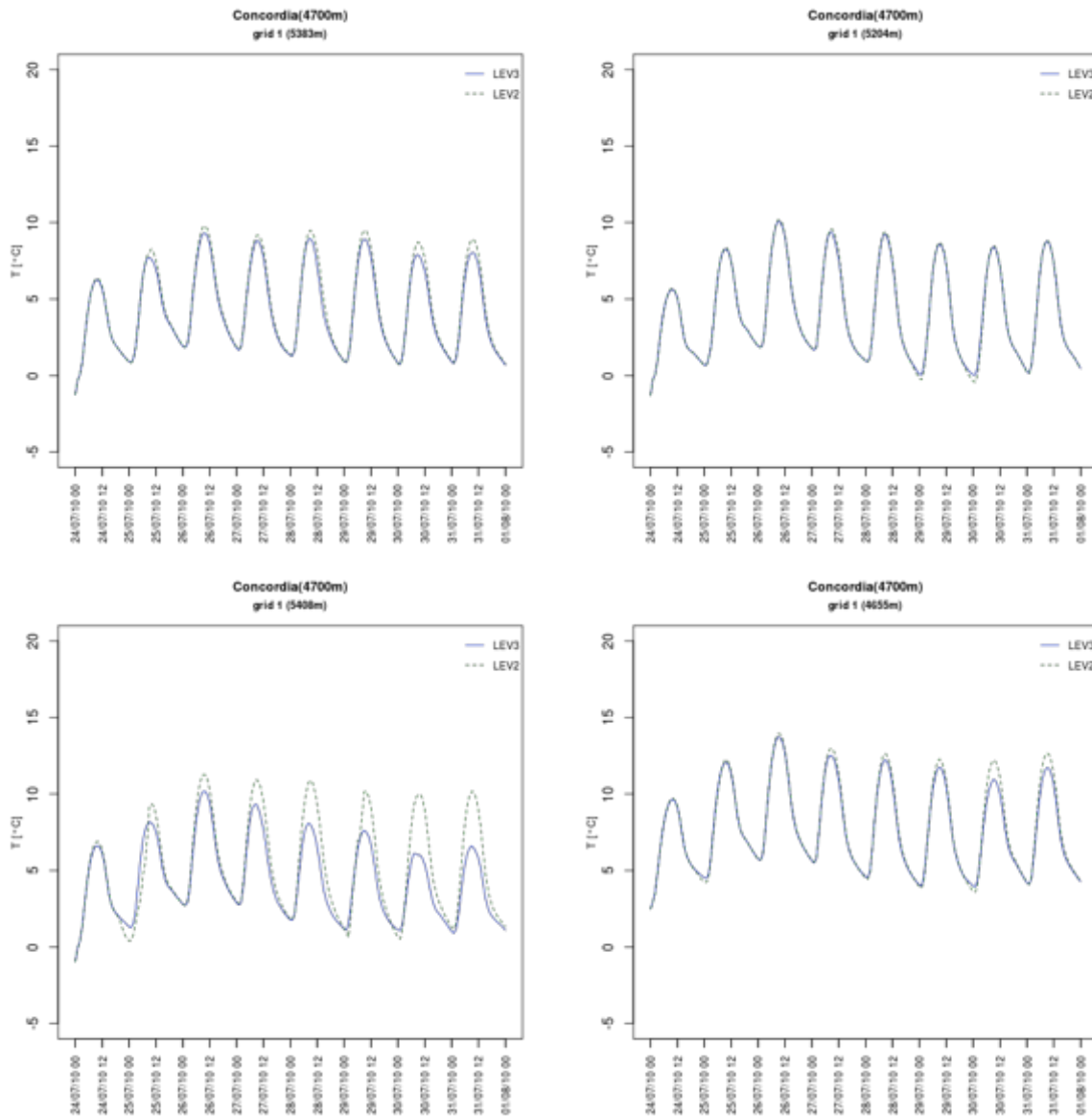


Fig. 2.10. Concordia station. Comparison between simulated temperature trends, using two different microphysics parameterizations, at the four nearest grid points for grid 1.

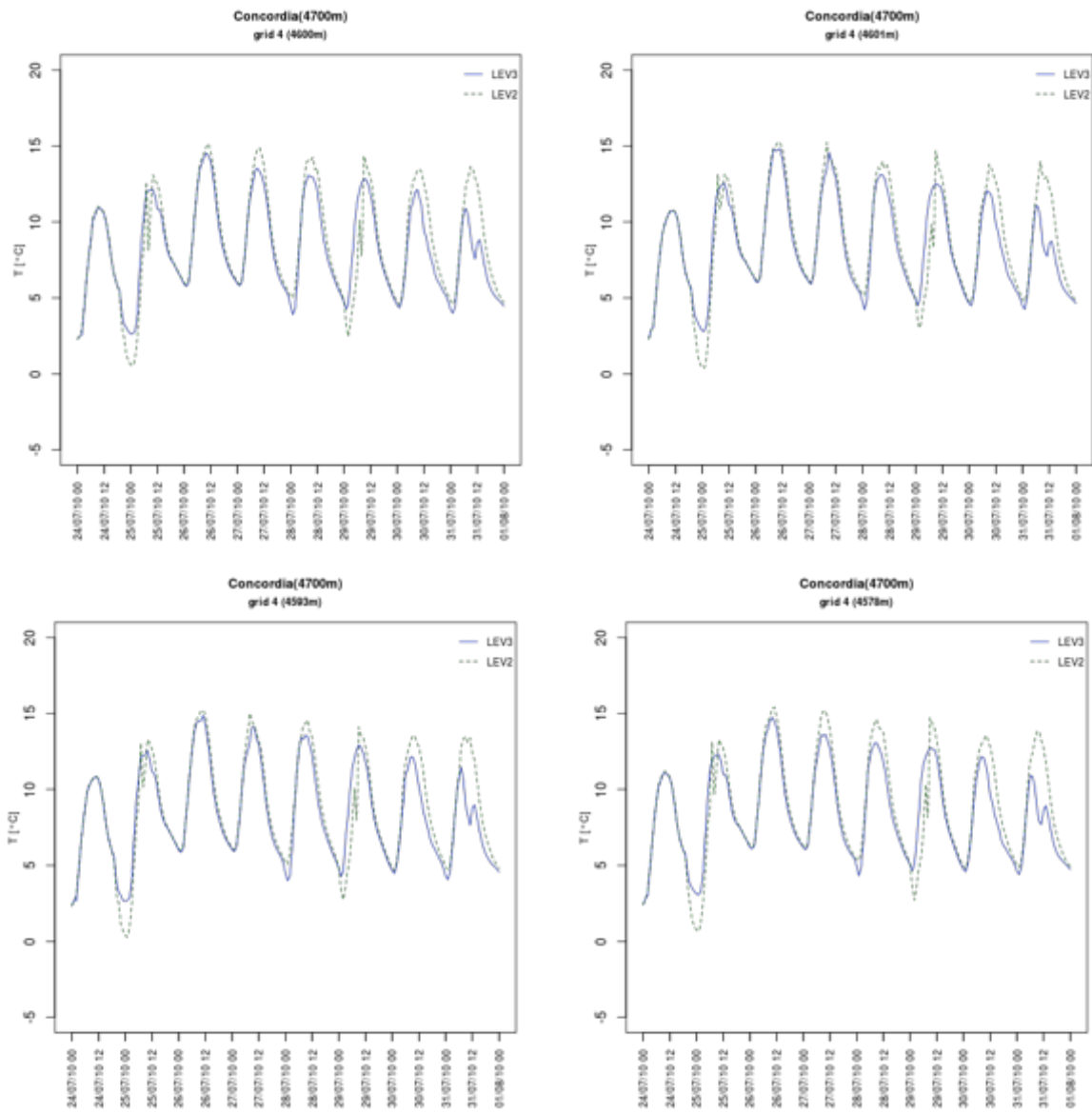


Fig. 2.11. Concordia station. Comparison between simulated temperature trends, using two different microphysics parameterizations, at the four nearest grid points for grid 4.

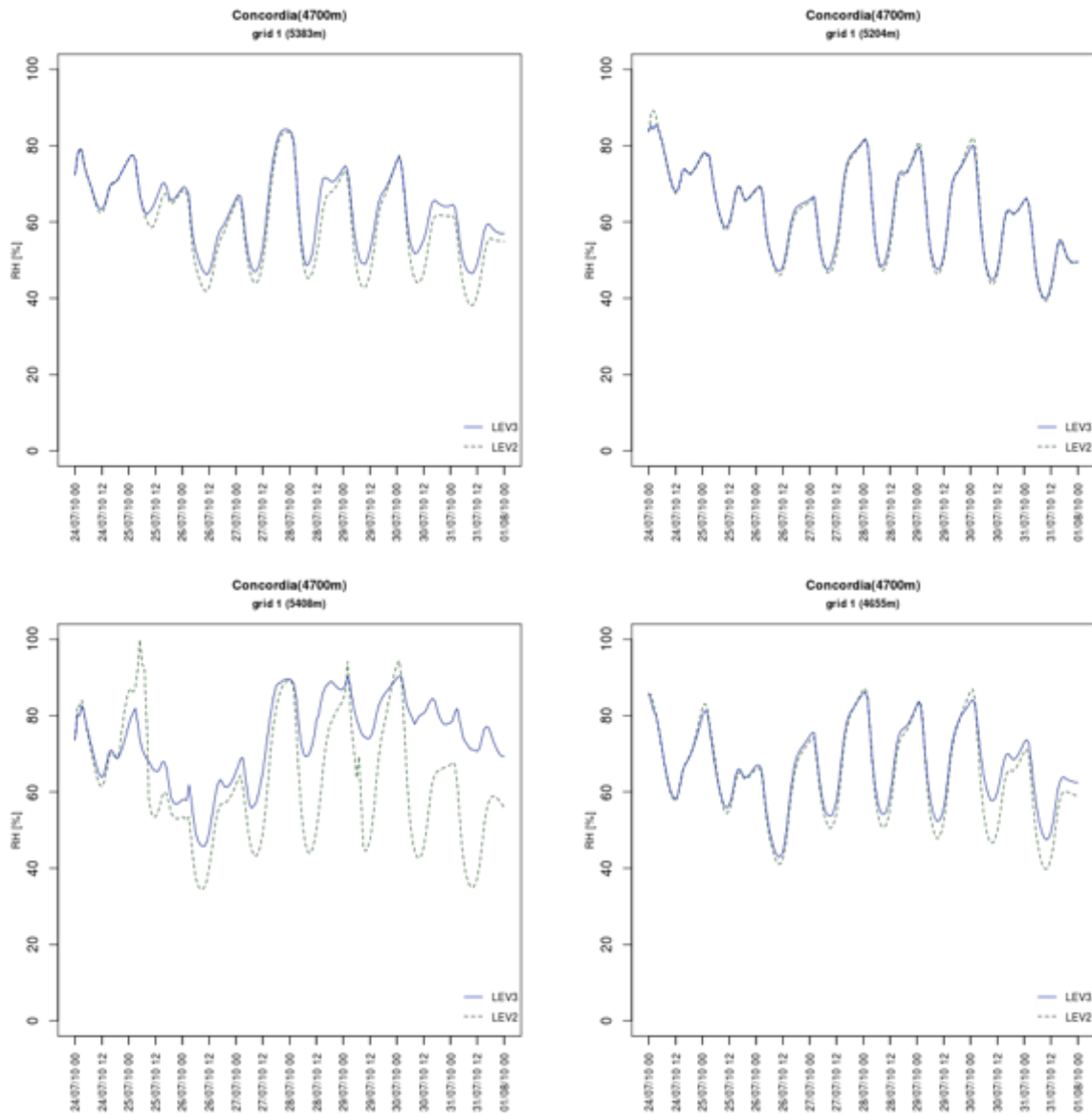


Fig. 2.12. Concordia station. Comparison between simulated relative humidity trends, using two different microphysics parameterizations, at the four nearest grid points for grid 1.

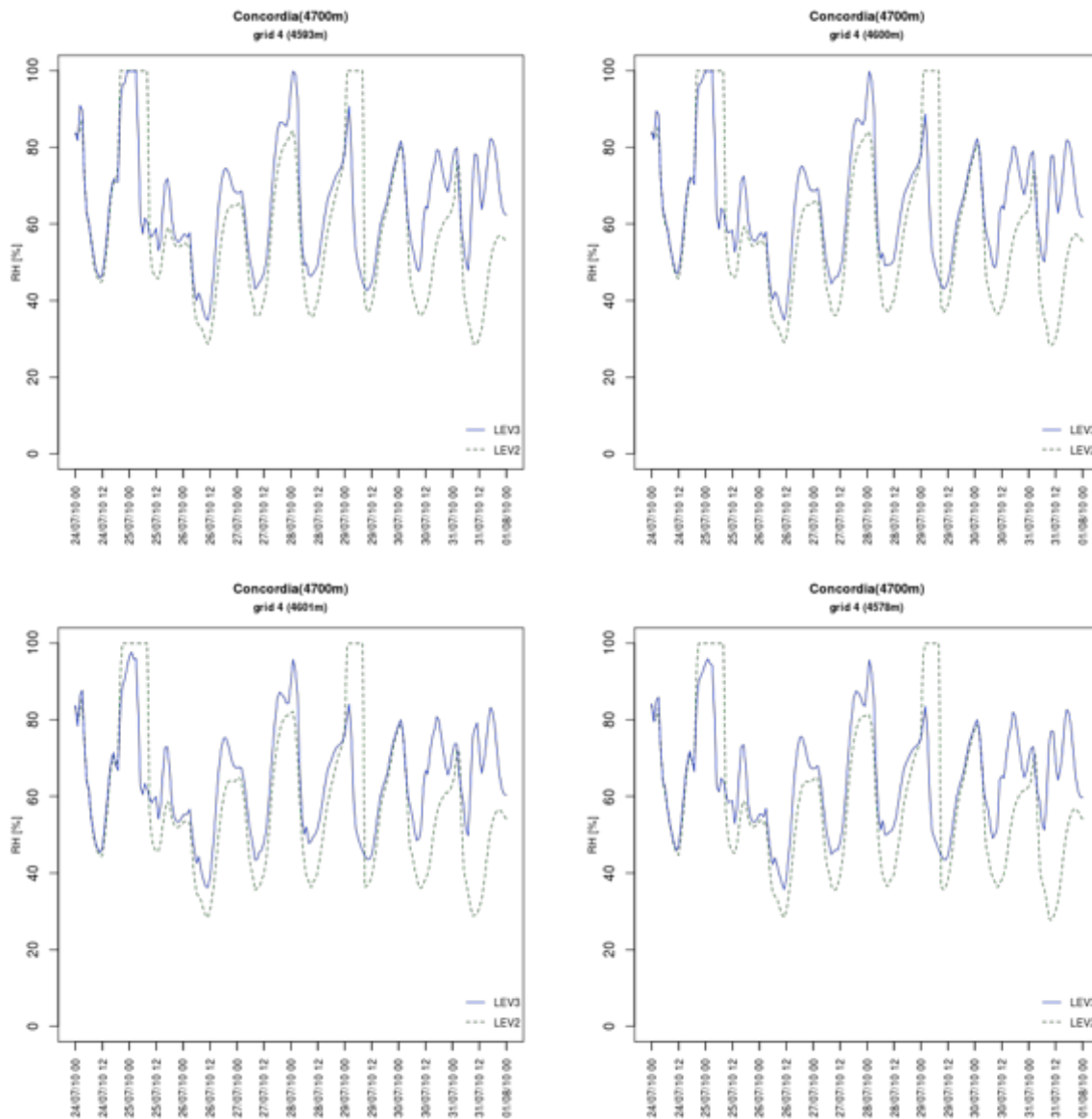


Fig. 2.13. Concordia station. Comparison between simulated relative humidity trends, using two different microphysics parameterizations, at the four nearest grid points for grid 4.

Generally, since only the microphysics parameterization is different in the two runs, the larger perturbations in the temperature and in the relative humidity occurring in the simulation for TestW_1 are to be linked to the intense precipitation event, occurring between the 29/07 and 01/08, as also shown in next Figures at PMD stations.

Comparisons have been carried out at the PMD stations because the measurements are available only for these stations and not for NextData stations. In particular, for each period, we compared the simulated temporal evolution of the temperature with the corresponding daily-observed maximum and minimum values, and the resolved surface precipitation, defined as “the average volume of water in the form of rain, snow, hail, or sleet that falls per unit of area and per unit of time at the site”, with their mean daily observed rainfall.

Also for the PMD stations, we extracted the simulated fields from analysis file at the four grid points around the station, SW, NW, SE and NE.

Regarding temperature and precipitation compared to the available observations, we report as example the plots for PMD stations, Astore, Skardu, Gilgit and Bunji, for grid 3. It was possible to extract the simulated values only for grid 3, because the stations coordinates are located outside the finest grid 4. In grid 3, the following cases take place:

1. the latitude of the stations Skardu and Bunji coincides with a latitude of the grid mesh, therefore only two grid-points where the longitudes are the closest to the station one, are considered;
2. the longitude of the stations Astore and Gilgit coincides with a longitude of the grid mesh, therefore only two grid-points where the latitudes are the closest to the station one, are considered.

In the next graphs, we compare simulated temperature trend against daily-observed maximum and minimum values and resolved surface precipitation trend against mean daily-observed values, respectively, at the four grid points around the studied station.

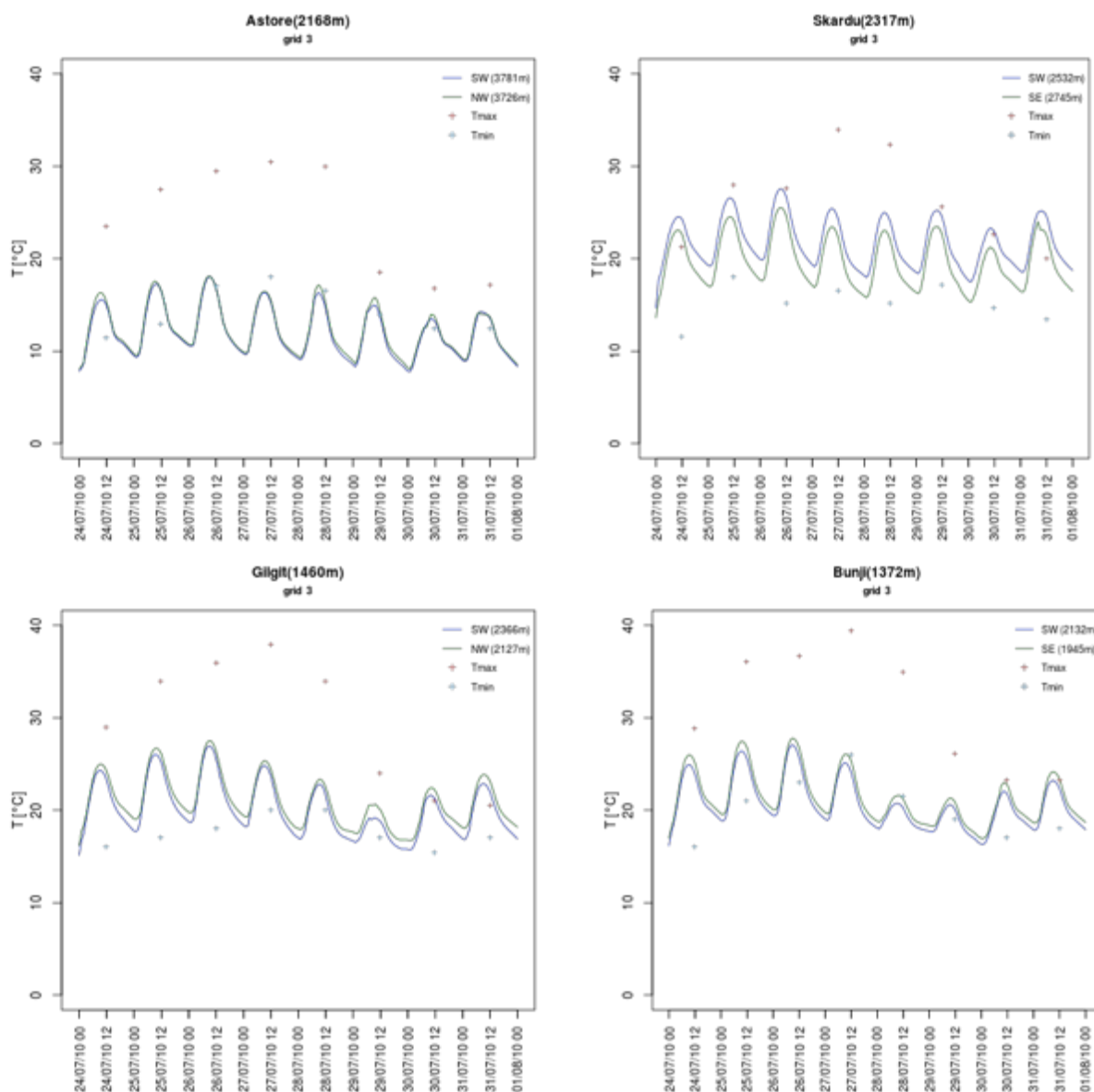


Fig. 2.14. Grid 3. Time evolution of the simulated temperature at the two grid points closest to the stations, compared to the corresponding observed daily maximum and minimum values: Astore, top left; Skardu, top right; Gilgit, bottom left; Bunji, bottom right.

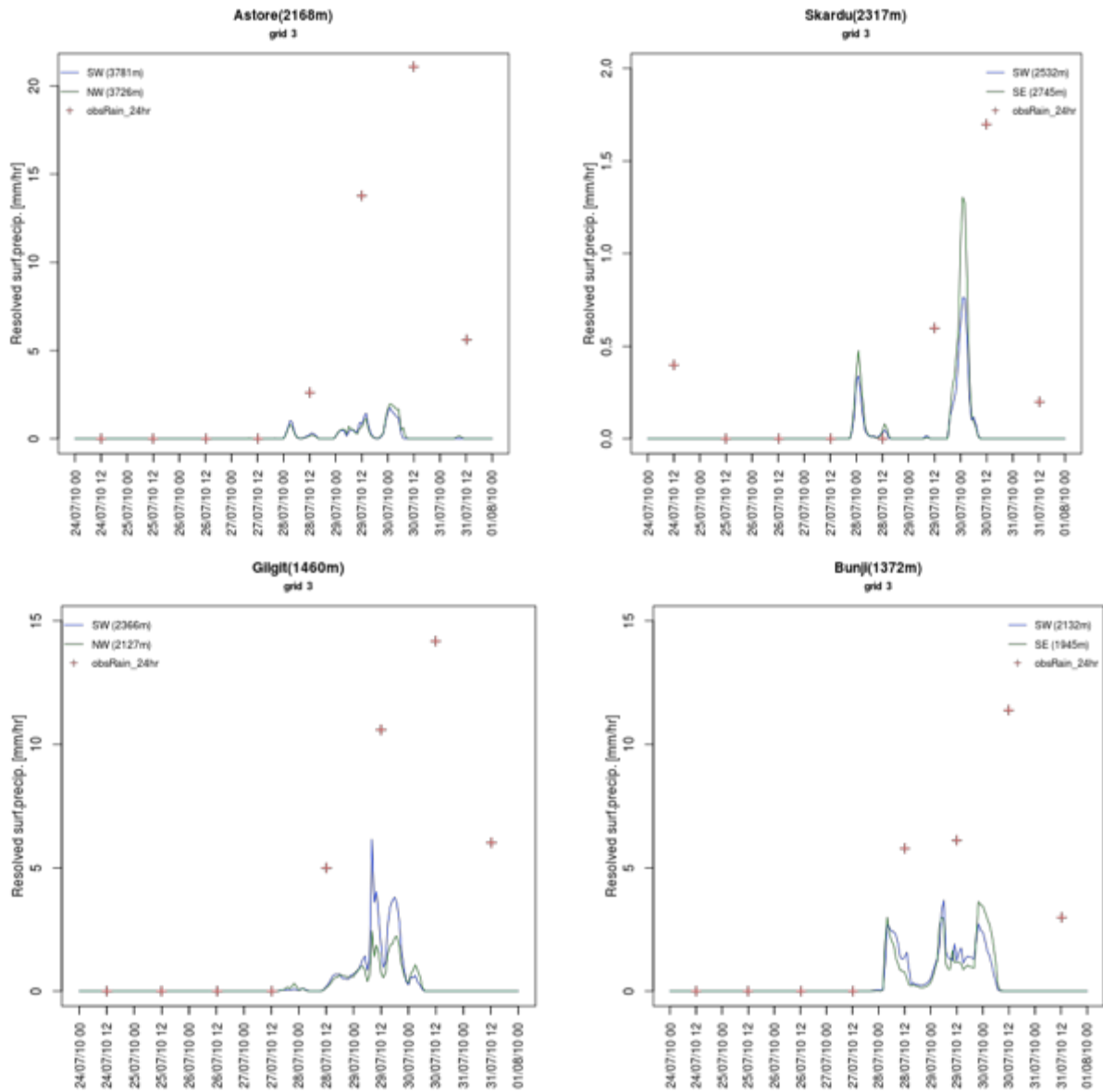


Fig. 2.15. Grid 3. Time evolution of the simulated precipitation at the two grid points closest to the stations, compared to the corresponding observed daily averages: Astore, top left; Skardu, top right; Gilgit, bottom left; Bunji, bottom right.

In Figure 2.14, for all stations we see that the temperature trend sets generally closer to the minimum observed values, getting far lower values than the maxima in the first five days, while in the last three ones, when the flood occurs, the agreement is better. Only for Skardu station, the agreement is fair. We notice, however, that the two grid-3 points close to Astore station, at 2168 m, have a much higher altitude, respectively 3781 m and 3726 m, resulting in more than 1500 m difference. Similar considerations hold for Gilgit (real altitude: 1460 m, grid points: 2366 m and 2127 m) and Bungji (real altitude: 1372 m, grid points: 2132 m and 1945 m) stations. Instead, the grid points around Skardu, 2317 m altitude, are placed at closer altitudes, 2532 m and 2745 m.

The differences in altitudes at the four PMD stations with respect to the grid points around them are certainly determining the different temperature values. This fact is better understood by looking at the position of the stations on maps (Figures 2.16-17-18), which highlight the extremely complex topography surrounding the stations themselves: in a range of 2 km radius, meteorological variables take certainly different values. Taking all this into account and given the relatively coarse horizontal resolution of grid 3, that is 4 km, the

predicted temperature daily evolution can be considered satisfactorily representative of the temperature in the area.

In Figure 2.15, the resolved surface precipitation at the two grid points is plot together with the observed mean-daily values at the four PMD stations. The comparison has to be taken in a qualitative way, since the two variables compared are not the same. The model correctly forecasts the intense precipitation event, in terms of period (last days of July), but it does not capture the observed mean, predicting lower values. In this case, the dislocation of the grid points with respect the actual position of the station may contribute to the difference, since precipitation is a rather local variable and may largely vary at distances of the order of 1 km. Generally, taking into account that the resolution for grid 3 is 4 km and the differences in altitude, the model results can be considered satisfactory. Since in previous simulations it was demonstrated that when increasing the resolution the meteorological variables at nearby grid points get closer values, the application of a mesoscale models at high resolution can provide reliable fields and an effective description of the local atmospheric circulation.

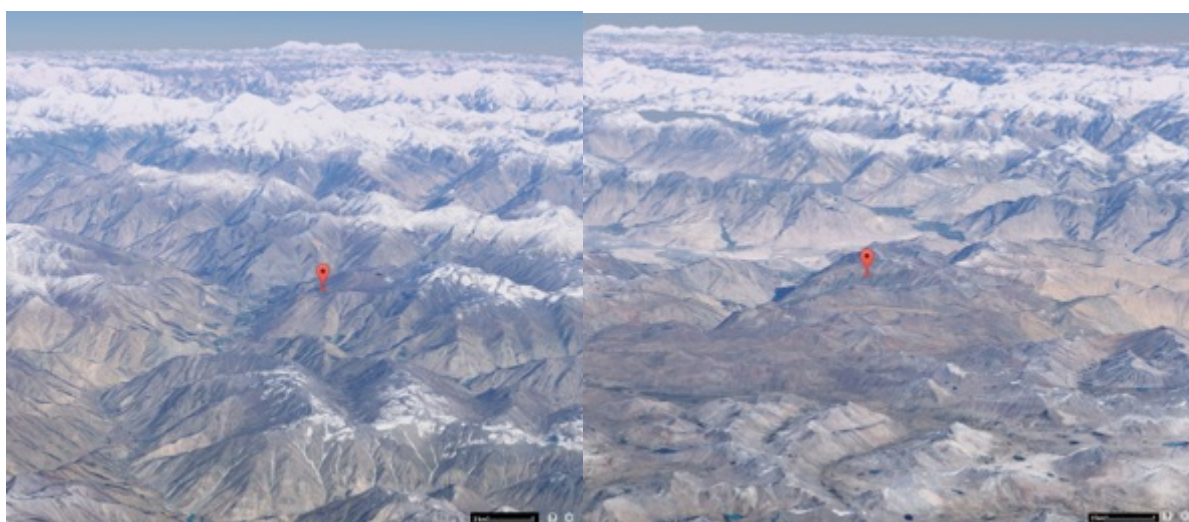


Fig. 2.16. Locations of Astore station (2168 m) on the left and Skardu station (2317 m) on the right.



Fig. 2.17. Gilgit station (1460 m) on the left and Bunji station (1372 m) on the right.



Fig. 2.18. PMD stations: Astore, Skardu, Gilgit and Bunji stations in red circles.

Numerical issues have been also evaluated, in order to investigate how much these aspects may influence the model outcome. In the next graphs, we compare results from the numerical tests for the one-week case. The tests were performed with reference to the Test_W1 case, using the same model configuration.

In Figures 2.19-2.21, we plot the comparison, at one grid point close to Concordia station, between the complete one-week simulation (24-31/07/2010) and a 36-hours simulation run in the same week (26-28/07/2010) targeted on the 27th of July, in order to test the effect of the spin-up time.

Regarding simulated temperature (Figure 2.19), the characteristic diurnal temperature cycle, reported for the entire day of 27th July, shows a good agreement between the two cases. What is noticeable is that the peak values for the 36-hours run are quite lower than for the one-week case one on July 27th. This is clearly connected to the “initial” conditions for the 36-hours run during the first hours of the simulation on July 26th, starting from a much lower temperature than the one predicted during the one-week case for the same day. The effect of the spin-up time is thus evident.

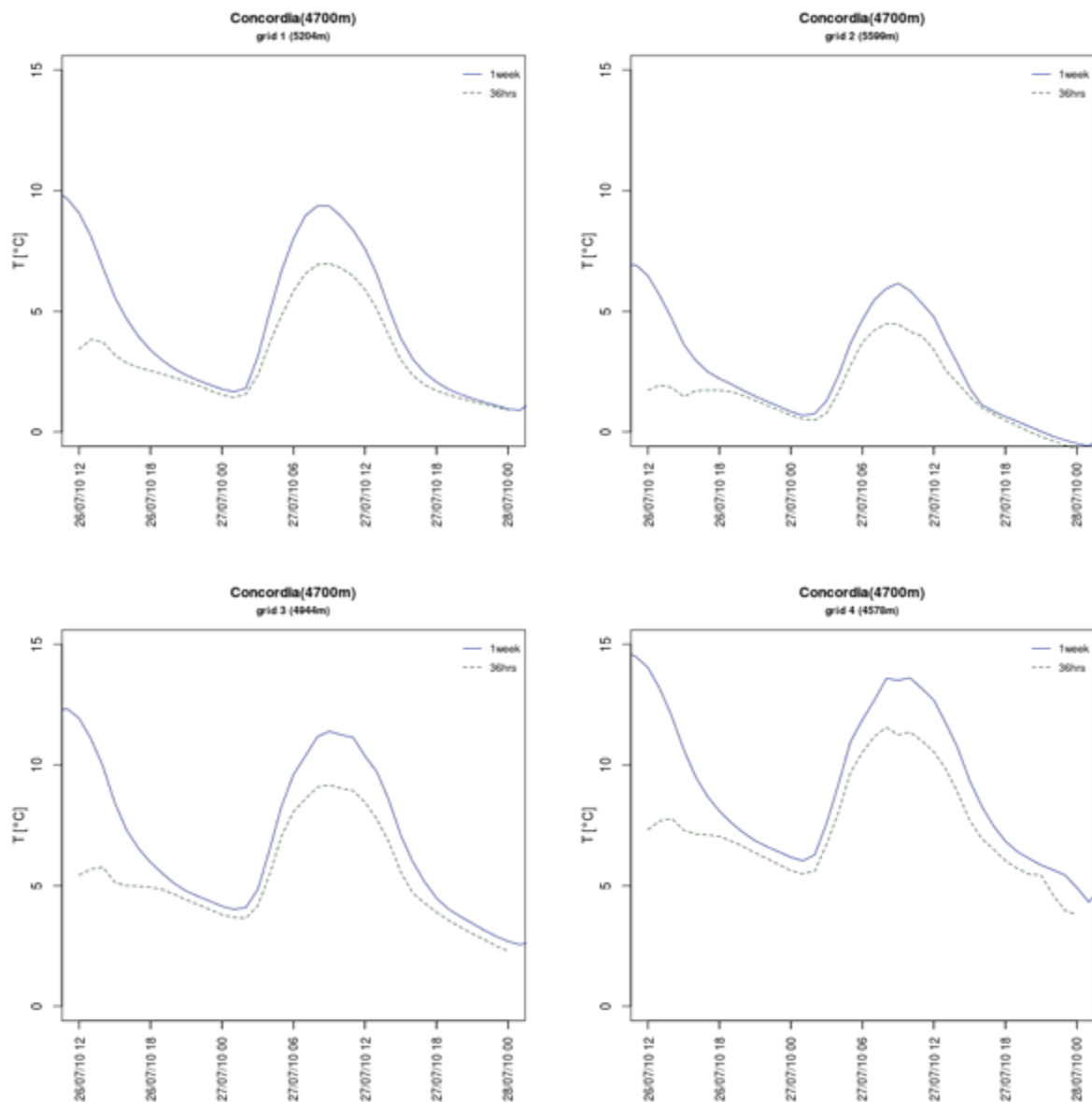


Fig. 2.19. Concordia station. Comparison between simulated temperature trends, for one-week case (blue line) and for a shorter 36-hours run (dashed green line), at one grid point and for all grids: grid 1, top left; grid 2, top right; grid 3, bottom left; grid 4, bottom right.

Concerning the simulated wind speed (Figure 2.20), we observe that the trends almost superpose for grid 1 and 2, with some time shift for the 36-hours curve in grid 2, and they have also a similar cycle for grids 3 and 4. The 36-hours curve shows some more fluctuations and have a bit lower values than for the one-week case. The effect of the initial conditions due to the different spin-up periods can be appreciated also for the wind speed.

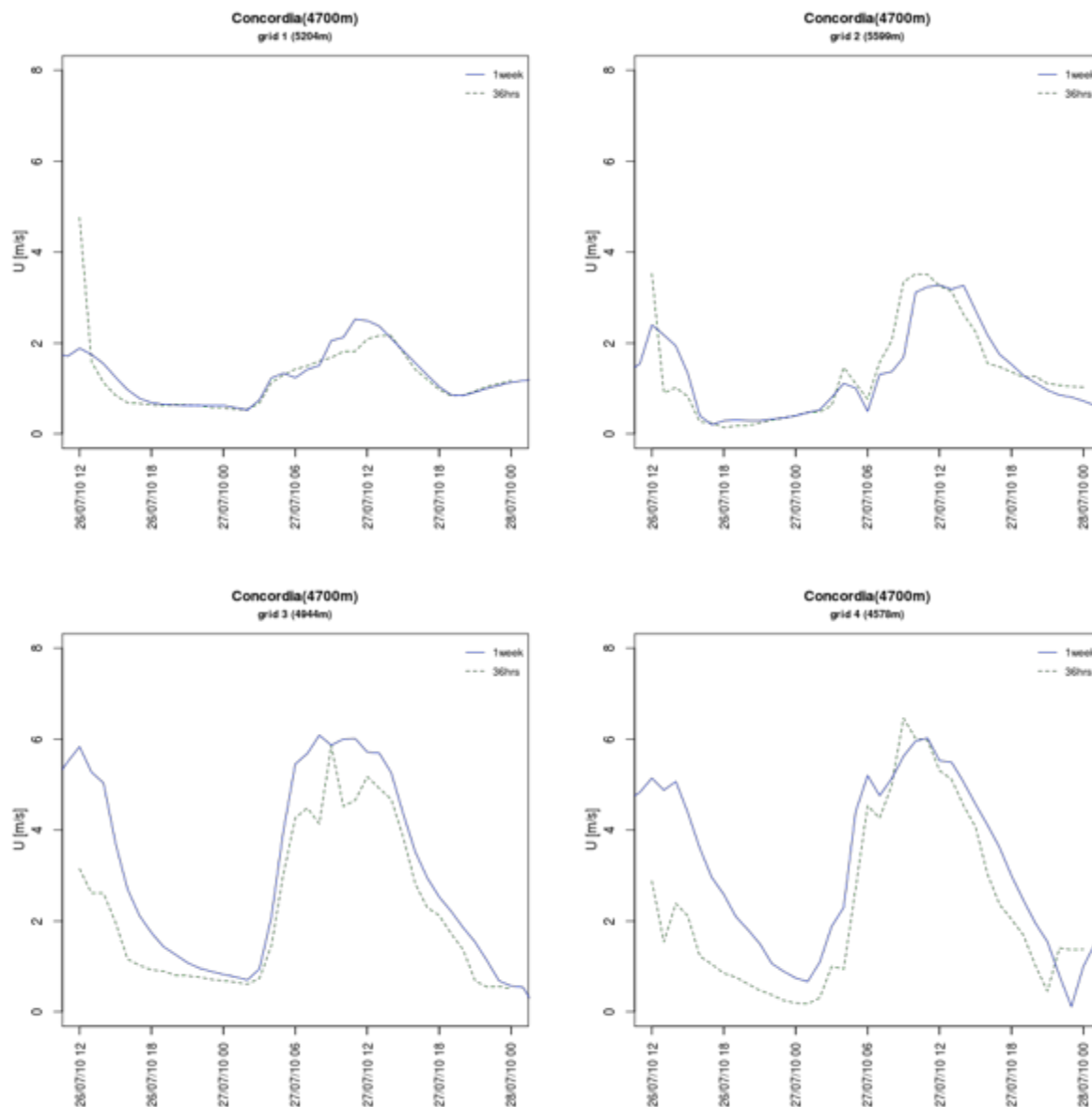


Fig. 2.20. Concordia station. Comparison between simulated wind speed trends, for one-week case (blue line) and for a shorter 36-hours run (dashed green line), at one grid point and for all grids: grid 1, top left; grid 2, top right; grid 3, bottom left; grid 4, bottom right.

The effect is more enhanced for the relative humidity, for which the model outputs get consistently different (Figure 2.21). The computed trends are very different: the 36-hours simulation predict values higher than in the one-week case and it does not well reproduce the diurnal pattern of humidity, which is instead depicted for the one-week run.

This analysis highlights the importance of the spin-up time for bringing the numerical simulation at a reliable operating configuration.

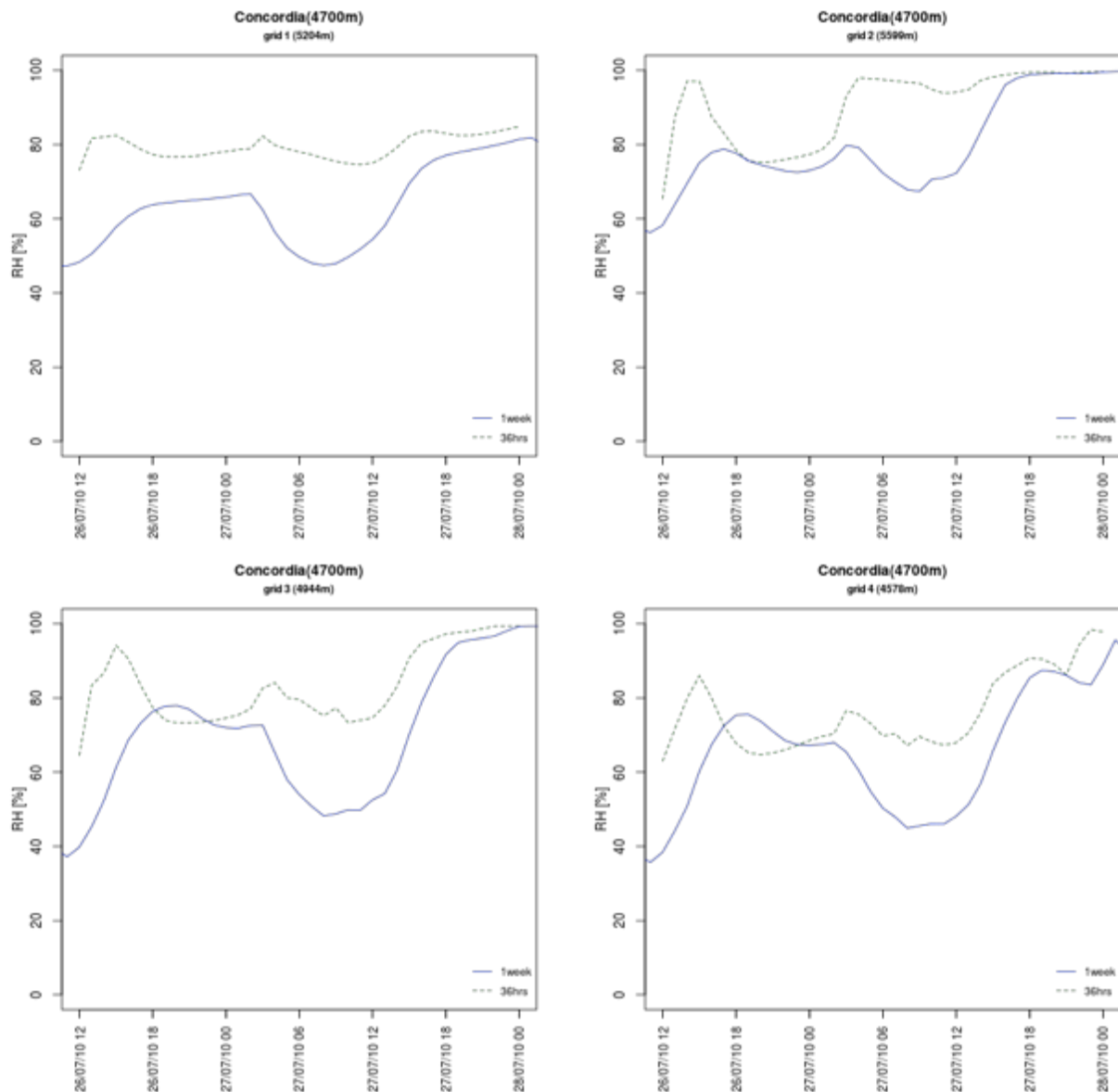


Fig. 2.21. Concordia station. Comparison between simulated relative humidity trends, for one-week case (blue line) and for a shorter 36-hours run (dashed green line), at one grid point and for all grids: grid 1, top left; grid 2, top right; grid 3, bottom left; grid 4, bottom right.

Lastly, we report the results of the “irregular” simulation from 24 to 31 July 2010 during which the RAMS run type option “HISTORY” has been used. An interruption of the run was simulated in order to test the way in which the model is to be restarted using the output files previously recorded, at the time of the break point. It means that the atmospheric and soil prognostic variables are read from an analysis state file, which was written by the model on a previous run, before the interruption or, as in our case, at the hour in which the model has been “virtually” stopped, that is on July 26th 2010 at 9:00 UTC.

In the next graphs, for TestW_1 case, we compare the numerical test results of the “restart” run against the one-week case, corresponding to the complete “continuous” simulation.

In Figures 2.22-24, we plot respectively the comparison between the temperature, wind speed and relative humidity for the week simulation (24-31/07/2010, blue curve) and the interrupted simulation (red curve) simulating the same week, in order to evaluate the effect of the restart option on the meteorological variables.

Concerning the simulated temperature (Figure 2.22), the two simulated trends are in good agreement for grid 1 and almost superpose for grid 2. Instead, for grid 3 and 4, two trends start differentiating at the break-point hour, at which the model has been “history” restarted.

The behaviour differs in the two grids, providing respectively higher and lower values for grid 3 and grid 4 with the restart run.

The differences between the simulated wind speeds are reported for all four grids in Figure 2.23: the curves diverge especially in grid 1 where the “restart” simulation predicts higher values than one-week simulation. Differences are shown also for the finer grids, but less marked.

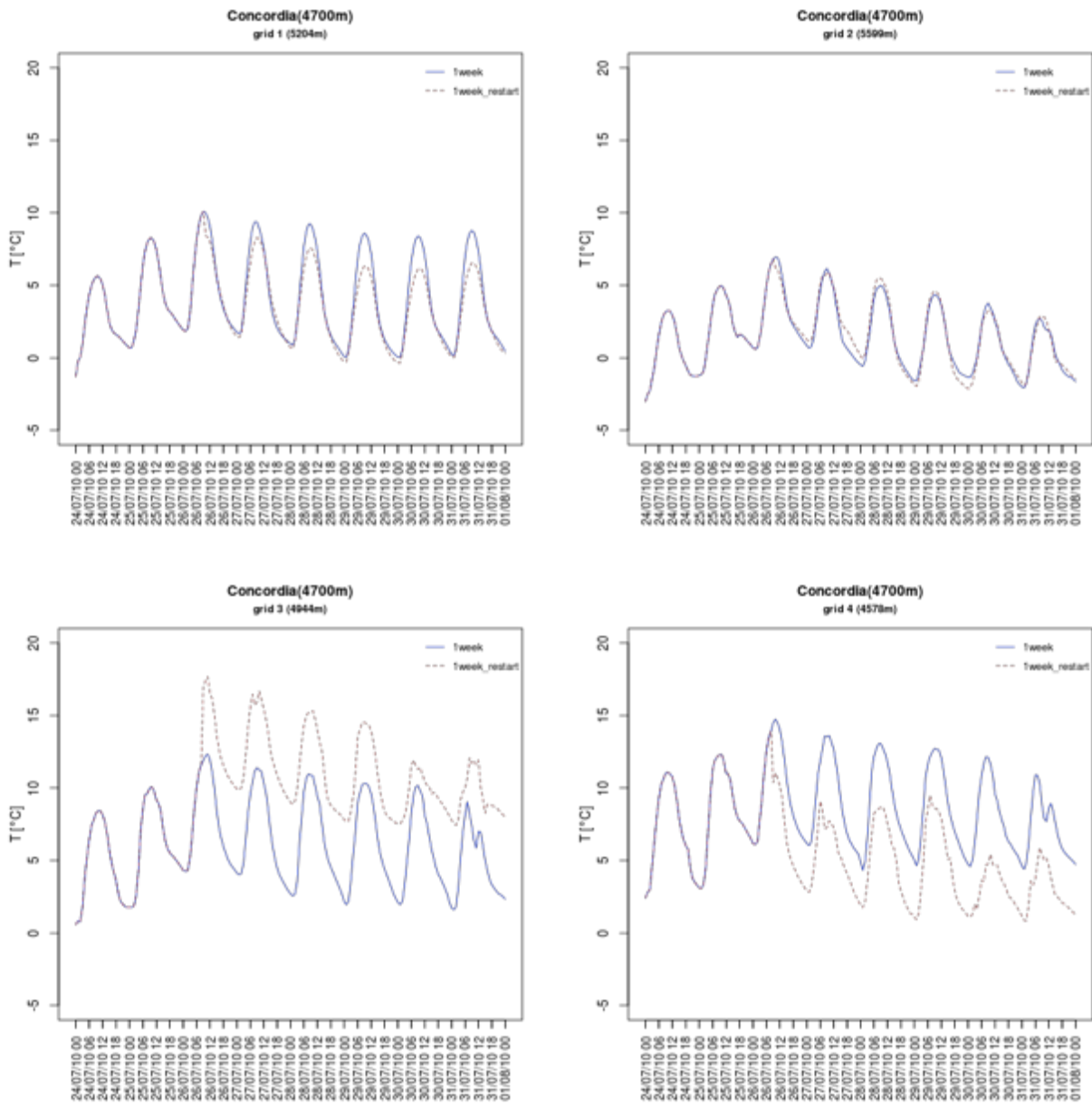


Fig. 2.22. Comparison between simulated temperature trends, for one-week case (blue curve) and for a “restart” procedure run (red curve), at one grid point close to Concordia station, for all grids.

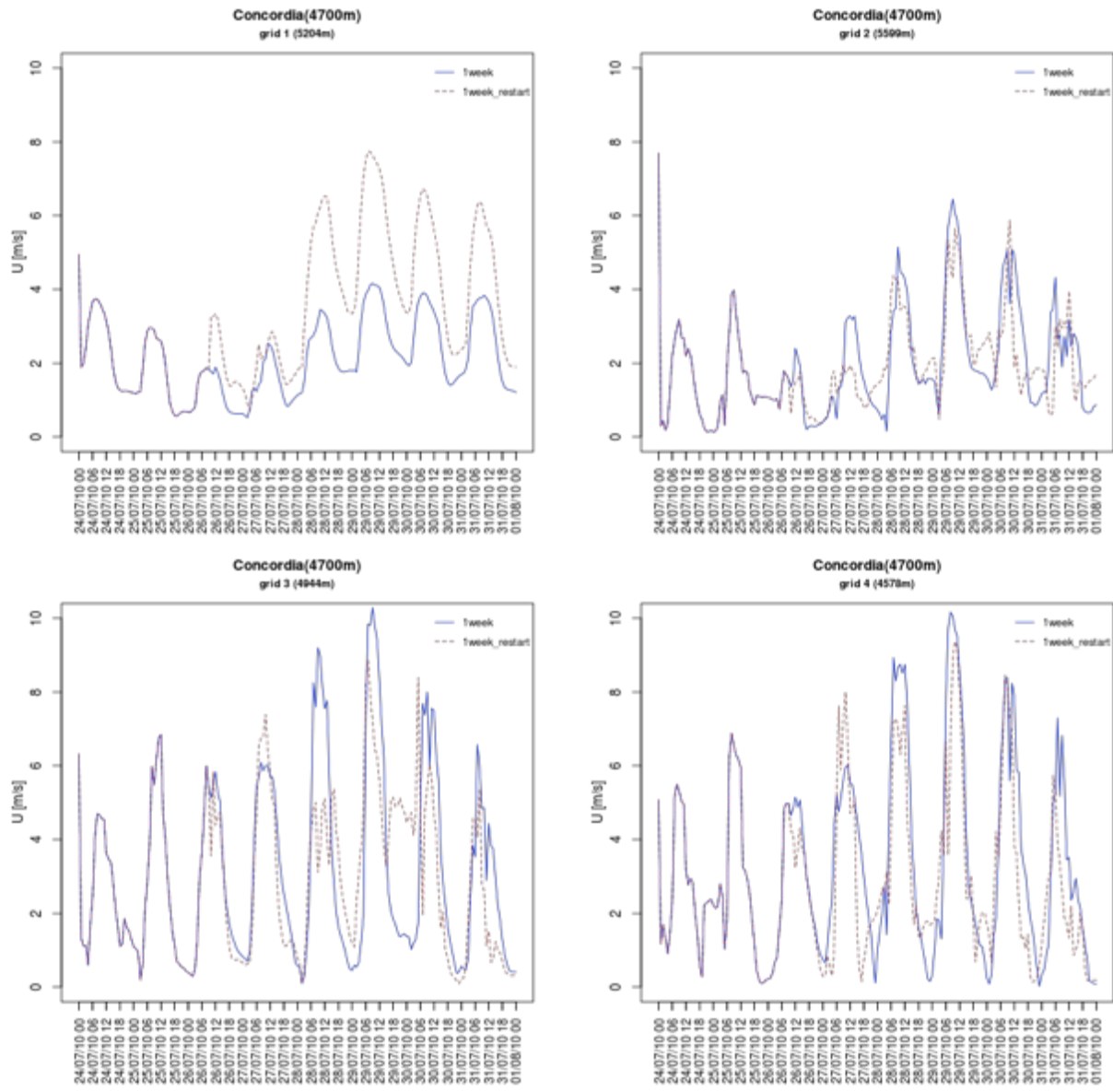


Fig. 2.23. Comparison between simulated wind speed trends, for one-week case (blue curve) and for a “restart” procedure run (red curve), at one grid point close to Concordia station, for all grids.

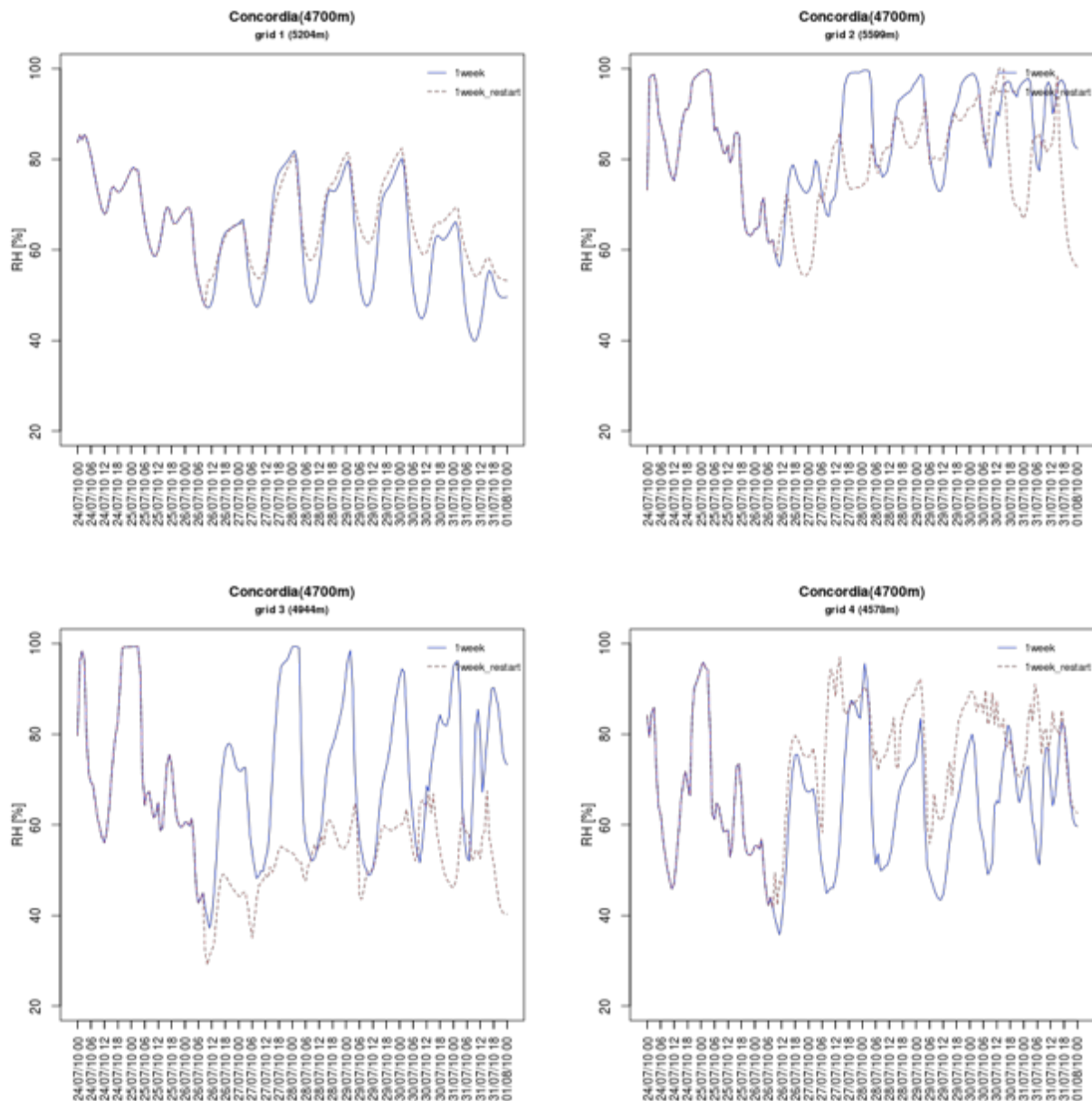


Fig. 2.24. Comparison between simulated relative humidity trends, for one-week case (blue curve) and for a “restart” procedure run (red curve), at one grid point close to Concordia station, for all grids.

Regarding the relative humidity (Figure 2.24), the simulated trends are very different in grid 2, 3 and 4. In particular, in grid 3, the “restart” simulation values are lower than the one-week ones, starting from the time at which the interruption occurred; in grid 4, there is instead an opposite tendency. It is difficult to provide an interpretation of this behaviour, in particular considering that the two simulations do not differ always in the same way for each variable at all grids. Surely, it is connected to the change in the (re)initialization of the runs as also supported by the 36-hours test, and this needs further investigation. The clear message is that using the restart option that is starting from an output analysis file, might lead to different results with respect to a uninterrupted simulation.

The conclusions related to the numerical tests performed for TestW_1 case, can be summarized as (1) not negligible differences were found in the time development of the meteorological variables for a shorter spin-up time, as seen in the 36-hours test; (2) the output fields tend to diverge when operating with the model in the ‘restart’ procedure: in our knowledge, this aspect was not investigated before and needs a further in-depth analysis and thorough discussion, since it is a procedure commonly adopted.

2.3 Conclusions and foreseen work

RAMS modelling activities have been planned to perform high-resolution (cloud-resolving) simulations for specific complex topography areas and to investigate relevant physical and dynamical processes over the mountainous areas of the Italian Alps and the Hindu Kush-Karakorum-Himalaya (HKKH). This allowed identifying and discussing the critical aspects of performing simulation of the atmospheric circulation in very inhomogeneous topographical conditions. Both physical and numerical aspects have been considered and studied on the modelling point of view. The results have been analysed and evaluated also using available observations from the PMD databank.

RAMS model, applied at high resolution, up to 1 km for the smallest grid, proved to be a reliable tool for reproducing the atmospheric circulation and the meteorological variables in very complex orography and also in extreme conditions, like for the flood episode occurred in HKKH area in July 2010. The first of the objectives cited in the introduction has been achieved, proposing a sensitivity analysis that allowed addressing key physical and numerical issues related to simulations in highly complex terrain, at high resolutions.

This modelling activity will be continued in RECCO Project performing new simulations over the same domain (mountainous areas of the Hindu Kush-Karakorum-Himalaya, HKKH), but referring to another period, between 20/8/12 and 20/10/12. This foreseen work refers to the experimental campaign in PAPRIKA Project - *Cryospheric responses to Anthropogenic Pressures in the Hindu Kush Karakoram -Himalaya regions: impacts on water resources and Availability* - during which high-pollution episodes occurred and were studied. The rationale of the study is to assess the atmospheric conditions and provide high-resolution simulated fields of the meteorological variables that can be of support to investigate the flow dynamics and turbulence determining the air pollutant dispersion, to assess the air quality study and its relative impact assessment (e.g. valley circulation and long-range episodes, as mineral dust from Taklimakan). In fact, the atmospheric pollution involves a lot of physical processes and possible problems, related to the peculiarity of both meteorological and dispersive characteristics in complex topography. The mesoscale and local scale circulations, related to the presence of main and lateral valleys, ridges and land use heterogeneity (resulting in features such as air stagnation regions in the lee of obstacles, separation of the flow and differentially heated valley walls) superimpose over the large-scale circulation. Thus, to correctly reproduce the meteorology of the region of interest, also the forcing of the synoptic circulation has to be taken into account, possibly describing the interaction between the large-scale processes and the local and small-scale ones. This can be done through the nesting technique coupled with high-resolution domain meshes, downscaling from typical mesoscale to local scales.

Next, simulations over another domain in the Khumbu Valley (Nepal), located in the central part of the Himalayan range and including the area of Sagarmatha National Park, will be performed. Here, a network of Automatic Weather Stations provides data since 1994 at different altitudes. The main goal of this set of simulations is to better understand and interpret the transport processes in the valley, investigating the role of the mountain/valley circulation for the transport of pollutant between the boundary layer and the free atmosphere. The choice of the episodes of interest and related periods for the simulations, included in the period between 2006 and 2010, is still under evaluation.

REFERENCES

- ARNOLD D., MORTON D., SCHICKER I., SEIBERT P., ROTACH M. W., HORVATH K., DUDHIA J., SATOMURA T., MÜLLER M., ZÄNGL G., TAKEMI T., SERAFIN S., SCHMIDLI J., SCHNEIDER S.: High Resolution Modelling in Complex Terrain. Report on the *HiRCoT 2012* Workshop, Vienna, 21–23 February 2012.
- BROUSSEAU P., DESROZIERS G. and AUGER L., (2012): Recent research on AROME-France data assimilation. 22nd ALADIN workshop / HIRLAM All-Staff Meeting, Marrakech, 7 May 2012, http://www.cnrm.meteo.fr/aladin/spip.php?action=accéder_document&arg=2352&cle=52db87c940a8c96f1cb8cd65b51ca70589faf71&file=pdf%2FBrousseau_22AW_def.pdf.
- BUZZI M., (2008): Challenges in Operational Numerical Weather Prediction at High Resolution in Complex Terrain. On the atmospheric boundary layer over highly complex topography, Ph.D. thesis, ETH Zurich No. 17714, 196 pp., available at <http://ecollection.ethbib.ethz.ch/view/eth:30923>.
- CALHOUN D., and LEVEQUE R. J., (2000): A Cartesian grid finite volume method for the advection-diffusion equation in irregular geometries. *J. Comput. Phys.*, 157, 143-180.
- CAYA A., SUN J., SNYDER C., (2005): A Comparison between the 4DVAR and the Ensemble Kalman Filter Techniques for Radar Data Assimilation. *Mon. Wea. Rev.*, 133, 3081-3094.
- DURRAN, DALE R., (2010): Numerical Methods for Fluid Dynamics with Applications to Geophysics. Texts in Applied Mathematics, 32, Springer. ISBN-10: 1441964118.
- DE WEKKER S.F.J., STEYN D.G., FAST J.D., ROTACH M.W., ZHONG S., (2005): The performance of RAMS in representing the convective boundary layer structure in a very steep valley, *Environmental Fluid Mechanics* 5, 35-62.
- DHARSSI I., BOVIS K. J., MACPHERSON B., and JONES C. P., (2010): Assimilation of ASCAT surface soil wetness. Forecasting R&D Technical Report No. 548, Met Office, Exeter, UK.
- DHARSSI I., BOVIS K. J., MACPHERSON B., AND JONES C. P., (2011): Operational assimilation of ASCAT surface soil wetness at the Met Office. *Hydrol. Earth Syst. Sci.*, 15, 2729-2746, doi:10.5194/hess-15-2729-2011.
- DIMRI A.P., (2009): Impact of subgrid scale scheme on topography and landuse for better regional scale simulation of meteorological variables over the western Himalayas, *Clim. Dyn.*, 32, , 565-574, doi:10.1007/s00382-008-0453-z.
- DRAPER C., MAHFOUF J.-F., CALVET J.-C., MARTIN E., and WAGNER W., (2011): Assimilation of ASCAT near-surface soil moisture into the SIM hydrological model over France. *Hydrol. Earth Syst. Sci.*, 15, 3829-3841, doi:10.5194/hess-15-3829-2011.
- FAO/IIASA/ISRIC/ISSCAS/JRC, 2009: Harmonized World Soil Database (version 1.1). Rome, Italy and Laxenburg, Austria.
- FAROUX S., MASSON V., and ROUJEAN J.-L., (2007): ECOCLIMAP [land cover + surface parameters] database for meteorological applications. Available from www.cnrm.meteo.fr/gmapdoc/IMG/pdf_ECOCLIMAP-SURFEX.pdf
- FAROUX S., ROUJEAN J.-L., KAPTUÉ A., and MASSON V., (2009): The ECOCLIMAP-II land surface database over Europe. CNRM/ Météo France Tech. Note 86, 120 pp. Available from CNRM / Météo France, 42 Av. G. Coriolis, 31057 Toulouse CEDEX 01, France.
- GENDT G., DICK G., REIGBER C., TOMASSINI M., LIU Y., and RAMATSCHI M., (2004): Near real time GPS water vapor monitoring for numerical weather prediction in Germany. *Journal of the Meteorological Society of Japan*, 82(1B), 361-370.
- GOHM A., ZÄNGL G. and GEIER G., (2004): South Foehn in the Wipp Valley on 24 October 1999 (MAP IOP 10): Verification of High-Resolution Numerical Simulations with Observations. *Mon. Wea. Rev.*, 132, 78-102.
- HAN X., LI X., HENDRICKS FRANSSEN H. J., VERECKEN H., and MONTZKA C., (2012): Spatial horizontal correlation characteristics in the land data assimilation of soil moisture, *Hydrol. Earth Syst. Sci.*, 16, 1349-1363, doi:10.5194/hess-16-1349-2012.

- HUANG X.-Y., XIAO Q., BARKER D.M., ZHANG X., MICHALAKES J., HUANG W., HENDERSON T., BRAY J., CHEN Y., MA Z., DUDHIA J., GUO Y., ZHANG X., WON D.-J., LIN H.-C., KUO Y.-H., (2009): Four-Dimensional Variational Data Assimilation for WRF: Formulation and Preliminary Results. *Mon. Wea. Rev.*, 137, 299-314.
- HONG S.-Y., and DUDHIA J., (2012): Next-generation numerical weather prediction: Bridging parameterization, explicit clouds, and large eddies. Meeting Summaries. *Bull. Amer. Meteor. Soc.* 93, ES6-ES9.
- JANJIC Z. I., GERRITY J. P., NICKOVIC S., (2001): An Alternative Approach to Nonhydrostatic Modelling. *Mon. Wea. Rev.*, 129, 1164–1178. doi:10.1175/1520-0493(2001)129<1164:AAATNM>2.0.CO;2
- KOSTER R.D., DIRMEYER P.A., GUO Z.C., BONAN G., CHAN E. (more), (2004): Regions of strong coupling between soil moisture and precipitation. *Science*, 305.
- LEUNG L. R., and S. J. GHAN, (1995): A subgrid parameterization of orographic precipitation. *Theor. Appl. Climatol.*, 52, 95–118.
- MAILHOT J., BENOIT R., (1982): A Finite-Element Model of the Atmospheric Boundary Layer Suitable for Use with Numerical Weather Prediction Models. *J. Atmos. Sci.*, 39, 2249– 2266. doi:10.1175/1520-0469(1982)039<2249:AFEMOT>2.0.CO;2.
- MAHANAMA S. P. P., KOSTER R. D., REICHLER R. H., and ZUBAIR L., (2008): The role of soil moisture initialization in subseasonal and seasonal streamflow predictability: A case study in Sri Lanka. *Adv. Water Resour.*, 31, 1333–1343, doi:10.1016/j.advwatres.2008.06.004.
- MASSART S., PAJOT B., PIACENTINI A., and PANNEKOUCKE O., (2010): On the Merits of Using a 3DFGAT Assimilation Scheme with an Outer Loop for Atmospheric Situations Governed by Transport. *Mon. Wea. Rev.*, 138, 4509-4522.
- MAXWELL R.M., CHOW F.K., and KOLLET S.J., (2007): The groundwater–land-surface– atmosphere connection: Soil moisture effects on the atmospheric boundary layer in fullycoupled simulations, *Advances in Water Resources*, 30, 2447-2466, doi:10.1016/j.advwatres.2007.05.018.
- MITTAL R., and IACCARINO G., (2003): Immersed boundary methods. *Annu. Rev. Fluid Mech.*, 37, 239-261.
- PORTER A.R., ASHWORTH M., GADIAN A., BURTON R., CONNOLLY P., BANE M., (2010): WRF code Optimisation for Meso-scale Process Studies (WOMPS) dCSE Project Report. (<http://www.hector.ac.uk/cse/distributedcse/reports/womps/womps.pdf>)
- ROTACH M.W. and ZARDI D., (2007): On the boundary layer structure over highly complex terrain: key findings from MAP, *Quarterly J. Roy. Meteorol. Soc.*, 133, 937–948, DOI: 10.1002/qj.71.
- ROTACH M.W., ANDRETTA M., CALANCA P., WEIGEL A.P., WEISS A., (2008): Turbulence characteristics and exchange mechanisms in highly complex terrain, *Acta Geophysicae*, 56 (1), 194-219.
- ROTACH M.W., CALANCA P., GRAZIANI G., GURTZ J., STEYN D.G., VOGT R., ANDRETTA M., CHRISTEN A., CIESLIK S., CONNOLLY R., DE WEKKER S.F.J., GALMARINI S., KADYGROV E.N., KADYGROV V., MILLER E., NEININGER B., RUCKER M., VAN GORSEL E., WEBER H., WEISS A., ZAPPA M., (2004): Turbulence structure and exchange processes in an Alpine Valley: The Riviera project, *Bulletin of the American Meteorological Society*, 85 (9), 1367-1385, DOI:10.1175/BAMS-85-9-1367.
- SATOMURA T., IWASAKI T., SAITO K., MUROI C., and TSUBOKI K., (2003): Accuracy of terrain following coordinates over isolated mountain: Steep mountain model intercomparison project (St-MIP). *Annals Disaster Prevention Res. Inst.*, 46B, 337-346.
- STEPPELER J., BITZER H.-W., MINOTTE M., and BONAVENTURA L., (2002): Nonhydrostatic atmospheric modelling using a z-coordinate representation. *Mon. Wea. Rev.*, 130, 2143–2149.
- TERMONIA P., DECKMYN A. and HAMDY R., (2009): Study of the Lateral Boundary Condition Temporal Resolution Problem and a Proposed Solution by Means of Boundary Error Restarts. *Mon. Wea. Rev.*, 137, 3551-3566.
- TRINI CASTELLI S., FERRERO E. and ANFOSSI D., (2001): Turbulence Closures in neutral boundary layers over complex terrain, *Boundary-Layer Meteorology*, Vol. 100, 405–419.

- TRINI CASTELLI S., MORELLI S., ANFOSSI D., CARVALHO J. and ZAULI SAJANI S., (2004): Intercomparison of Two Models, ETA and RAMS, with TRACT Field Campaign Data. *Environmental Fluid Mechanics*, 4, 157–196.
- TRINI CASTELLI S., HARA T., OHBA R. and TREMBACK C.J., (2006): Validation studies of turbulence closure schemes for high resolutions in mesoscale meteorological models. *Atm. Environment* 40, 2510–2523.
- TRINI CASTELLI S., and REISIN T. G., (2011): Application of a modified version of RAMS model to simulate the flow and turbulence in the presence of buildings: the MUST COST732 exercise. *Int. J. Environment and Pollution*, 44 (Nos. 1/2/3/4), 394-402.
- TRINI CASTELLI S., BELFIORE G. and ANFOSSI D., (2011): Modelling the meteorology and traffic pollutant dispersion in highly complex terrain: the ALPNAP Alpine Space Project. *Int. J. Environment and Pollution*, Vol. 44 (Nos. 1/2/3/4), 235-243.
- TSENG Y.-H., and FERZIGER J. H., (2003): A ghost-cell immersed boundary method for flow in complex geometry. *J. Comput. Phys.*, 192, 593-623.
- WAGNER W., HAHN S., KIDD R., MELZER T., BARTALIS Z., HASENAUER S., FIGA J., DE ROSNAY P., JANN A., SCHNEIDER S., KOMMA J., KUBU G., BRUGGER K., AUBRECHT C., ZÜGER J., GANGKOFNER U., KIENBERGER S., WANG Y., BLÖSCHL G., EITZINGER J., STEINNOCHER K., ZEIL P., RUBEL F., (2012, submitted): The ASCAT Soil Moisture Product: Specifications, Validation, Results, and Emerging Applications. *Meteorologische Zeitschrift*.
- WALKO R.L., AVISSAR R. (2008): OLAM: Ocean-Land-Atmosphere Model - Model Input Parameters - Version 3.0. Tech. Rep., Duke University.
- WYNGAARD J.C., (2004): Toward numerical modelling in the 'terra incognita'. *J. Atmos. Sci.* 61, 1816-1826.
- YAMAZAKI H., and SATOMURA T., (2008): Vertically combined shaved cell method in a zcoordinate nonhydrostatic atmospheric model. *Atmos. Sci. Lett.*, 9, 171-175.
- YAMAZAKI H., and SATOMURA T., (2010): Nonhydrostatic Atmospheric Modelling Using a Combined Cartesian Grid. *Mon. Wea. Rev.*, 138, 3932-3945.
- YAMAZAKI H., and SATOMURA T., (2012): Non-hydrostatic atmospheric cut cell model on a block-structured mesh. *Atmos. Sci. Lett.*, 13.(doi: 10.1002/asl.358).
- YE T., MITTAL R., UDAYKUMAR H. S., and SHYY W., (1999): An accurate Cartesian grid method for viscous incompressible flows with complex immersed boundaries. *J. Comput. Phys.*, 156, 20.
- ZÄNGL G., (2002): An improved method for computing horizontal diffusion in a sigma-coordinate model and its application to simulations over mountainous topography. *Mon. Wea. Rev.*, 130, 1423-1432. 9-240.
- ZÄNGL G., GOHM A., and GEIER G., (2004): South foehn in the Wipp Valley – Innsbruck region: Numerical simulations of the 24 October 1999 case (MAP-IOP 10). *Meteorol Atmos Phys* 86, 213–243, DOI 10.1007/s00703-003-0029-8.